Chapter 3
In-situ Transmission Electron Microscopy

Xiao Feng Zhang

Abstract Transmission electron microscopy (TEM) has hit a significant milestone of sub-angstrom resolution. On one hand, electron microscopists and materials scientists are enjoying the highest TEM spatial resolution ever attainable; on the other hand, study of materials in a steady state is hard to meet the increasing demand in new application fields such as nanocatalysts, nanocrystal growth, nanoelectronics, nanosensors, and nanomechanics in which size effect and structural or property responses to stimuli from the surrounding environment are key information to learn. Special attention is thus paid to in-situ TEM. A great deal of effort in developing and improving electron microscopes and specimen holders have resulted in unprecedented progresses in attaining insight into materials in dynamic environments. In many ways, transmission electron microscopes are now functionalized as workstations or nanoscale labs rather than just imaging tools. In this chapter, various types of in-situ TEM technologies are introduced accompanied by application examples. In parallel to the sub-angstrom breakthrough made by the aberration-corrected TEM, atomic resolution is now emphasized in advanced in-situ TEM, advancement on this aspect will be discussed together with other important notes and further challenges.

3.1 What is the In-situ TEM and Why It Is Important

One of the milestones in materials characterization technology in the 20th century was the invention of the transmission electron microscope in 1931. Among many advantages of transmission electron microscopy (TEM) compared with other imaging technologies,

X. F. Zhang (✉)
Nanotechnology Systems Division, Hitachi High Technologies America, Inc.,
5960 Inglewood Drive, Suite 200, Pleasanton, CA 94588, USA
e-mail: xiao.zhang@hitachi-hta.com

X. F. Zhang
Hitachi High Technologies Corporation, Tokyo 105-8717, Japan

A. Ziegler et al. (eds.), *In-situ Materials Characterization*,
Springer Series in Materials Science 193, DOI: 10.1007/978-3-642-45152-2_3,

a distinctive and very unique one is the twofold structural information obtainable on the same instrument. Electron diffraction tells structural information in the reciprocal space just like what X-ray and neutron diffractions tell, and the real space TEM images reveal morphologies and atomic lattice structures of objects. Five decades later, instrumentation and TEM have been well advanced and also combined with spectrometers for chemical analysis. TEM has become indispensable in materials science especially in the study of individual sub-micron size objects (such as nanomaterials, precipitates, grain boundaries, biological cells, and molecules) and locally deformed structures (dislocations, stacking faults, and strained lattice). Because of the technical feasibility, conventional TEM has been focusing on stable structures in the electron microscope vacuum and at ambient temperature. However, since the main themes of today's materials science are moving to nanomaterials and energy-related materials, researches in catalysis, nanocrystal growth, solid/liquid/gas interactions, and gas sensing are largely stimulated. Accordingly, the demand for in-situ TEM capabilities is growing fast. "The electron microscope should be a workstation rather than only an imaging tool", this comment from Dr. David C. Joy of the Oak Ridge National Laboratory/USA draws a picture for what is happening in the field of in-situ TEM.

What is in-situ TEM? While there might exist various definitions, a definition given in a report entitled "Dynamic in-situ electron microscopy as a tool to meet the challenges of the nanoworld" prepared for National Science Foundation of the USA may serve as an excellent explanation [1]. In this report, in-situ TEM was defined as "*Some form of stimulus is applied to a sample while it is observed in a TEM*." According to this definition, in-situ TEM has two important characters, *stimulus* and *real-time observation*. Stimulus, or say an external field, needs to be applied directly to a TEM specimen sitting in an electron microscope column. Typical external fields used for in-situ TEM include heating, cooling, electric, magnetic fields, as well as mechanical forces (tensile, compressive) and ion beam irradiation. To apply an external field to the specimen area and perform TEM observation simultaneously, one just needs, in most cases, a specially designed TEM specimen holder and a transmission electron microscope, which allows the in-situ TEM specimen holder to fit in. Also, a fast image recording system (for example a video recorder or TV rate CCD camera) is important. Sometimes, a modification of the transmission electron microscope is necessary. In this chapter, all these important facets of the in-situ TEM technology will be touched.

A question to ask is: why bother using in-situ TEM? Can't we simply treat materials ex-situ, say in a reaction chamber outside of an electron microscope and then move the treated sample back into the electron microscope for observation? One can certainly do the sample treatment/observation in this way, which is in fact one typical way of using TEM in the materials science field. But from ex-situ TEM experiments, only the beginning and ending status of materials can be learned. What has happened during the middle stages is missed. Misinterpretations of experimental data, wrong assumptions, or incorrect derivations were indeed not rare in reality when real-time observation capabilities were not available. A simple analog is crime scene investigation. For investigators who see the result of a criminal event, it is also not so difficult to learn about the scene before the crime. In order to figure

out what happened during the criminal activity, investigators would have to collect all information they could dig out such as finger prints, blood samples, and residues. As electron microscopists and materials scientists, we are fortunate to have a state-of-the-art in-situ TEM to reveal structural evolution in materials in real time when it happens. Another angle to look at why we need the in-situ TEM is that the capability of applying external fields or forces to the TEM specimens actually turns the TEM specimen chamber into a miniaturized laboratory in which chemical reactions, structures, or physical properties can be activated or altered at micrometer to nanometer scales and all of the processes are monitored at high spatial and temporal resolutions.

3.2 A Brief History of In-situ Microscopy

The invention of the transmission electron microscope was driven, in part, by a couple of disease mysteries encountered in late 19th century. People attributed the causes to some invisible living objects much smaller than bacteria, which were viruses as we know today. The size of viruses is 0.1 mm or smaller which is beyond the resolving power of the optical microscope, therefore no one could prove the existence of viruses in the late 19th to early 20th century despite all of the disease analyses pointed to its existence. Microscopes with much higher resolution were urgently needed. Concomitant with the invention of the first transmission electron microscope in 1931, three high expectations were put on this new, yet unproven microscope: Higher resolution than that of the optical microscope, good imaging contrast on biological samples, and observation of live objects. With a continuous development in 80 years, TEM resolution has been increased by 1000 times, from about 50 nm in the beginning to 0.05 nm on today's most powerful microscopes. In the meantime, imaging contrast for biological samples has also been significantly enhanced by allowing adjustment of the electron accelerating voltage, the focal length of the objective lens, the size of the objective aperture, and recently introducing phase-plate technology.

In contrast to the achievements in high resolution and high contrast imaging, progress in seeking solutions for live observation of biological specimens remains unsatisfied. Although electron microscopes have obvious advantages over optical microscopes in terms of high resolution and chemical analysis, the optical microscope allows looking at specimens in their original states and environments such as in air or liquid solution. Interestingly enough, live microscopy, or in-situ microscopy, can be traced back to more than 300 years ago. In 1679, Antoni Van Leeuwenhoek published his observations on live microbes using his home-made, one-lens microscope, Fig. 3.1 [2]. The discovery of these "my little animals" (nickname given by Van Leeuwenhoek) virtually opened a door for human beings toward the microworld. Since then, observing and studying biological systems in their live state has long been the highest interest of biologists and the same enthusiasm was naturally carried over to TEM observations in the mid 20th century. However, a big hurdle was the vacuum condition in the electron microscope column. The high vacuum of $\sim 10^{-5}$ Pa in the specimen chamber prevents any live biological specimen to endure

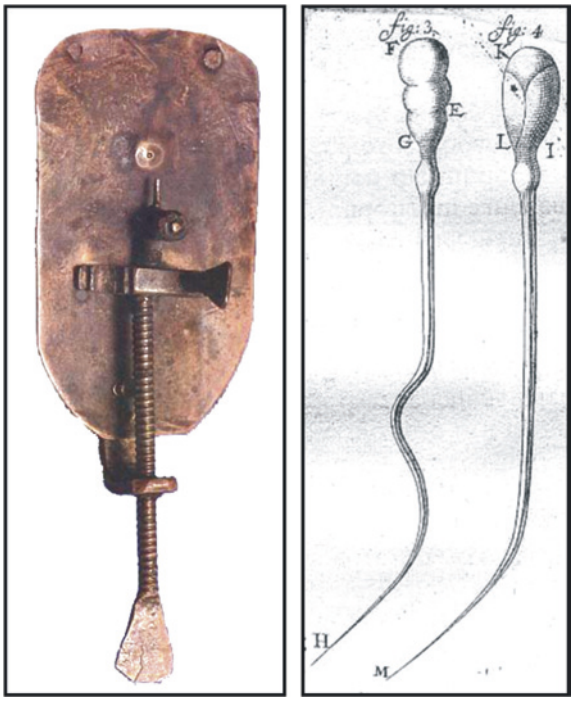

Fig. 3.1 In 1679, Antoni Van Leeuwenhoek published his observations on live sperms of a rabbit (*right*), using a simple one-lens microscope made by himself (*left*)

for a sufficient long time for electron microscopy study. The task was therefore pretty clear: gas or liquid solution or both must be introduced into the specimen area in the electron microscope. Such an ambient is not only beneficial to live observation of biological specimens, but also enables TEM studies on many other objects such as catalytic process/mechanism, material growth, and electrochemical process which require suitable gases or liquid solutions around specimens. In 1942, Ruska was probably the first to report a low vacuum transmission electron microscope for the purpose of providing a flexible environment to materials under TEM study [3]. In addition to the adjustable environment, external fields turned out to be crucial as well to mimic the real world conditions inside electron microscope chambers. Today, supplying gas or liquid solution to the specimen chamber of a transmission electron microscope is not a big challenge anymore. Also, by modifying TEM specimen holders, various holder-based in-situ TEM technologies have already matured and are widely used in materials science.

3.3 In-situ TEM Technologies

An important point the chapter author would like to make is that *to some extent,* in-situ *TEM is all about specimen holders*. Depending on what external field is to be applied to the specimen area, a corresponding specimen holder can be designed.

Most of the matured in-situ TEM technologies are based on elegant design of specimen holders like those used for in-situ heating, cooling, environmental, probe, straining, Lorentz, electron holography, and ion beam irradiation TEMs.

3.3.1 In-situ Heating and Cooling TEM

Perhaps the first in-situ heating TEM stage was reported in 1960 to observe annealing effects on dislocations in aluminum [4]. Nowadays, heating can be realized by placing a heating element at the tip of a TEM specimen holder. Depending on the heating element, heating mechanism, and sample fixing method, there are three typical types of commercially available in-situ heating TEM holders: furnace-heating holders, wire-heating holders, and membrane-heating holders. Joule heating of nanomaterials is also used in reported applications as will be described in Sect. 3.3.4.

At the tip of a furnace-heating holder, a heating filament embracing a 3 mm-diameter TEM specimen disk acts like an electric furnace. The thermal radiation heats the specimen, and is therefore an indirect heating mechanism. Cooling water is connected to the holder for use at above 500 °C. An embedded thermal couple measures temperature in the furnace cup. Because the 3 mm-diameter heating zone is "huge" and involves many components and supporting materials (e.g. TEM metal grid), the total thermal expansion effect causes a severe problem of sample drifting when changing temperature. It may take a few tens of minutes to seize the drifting, therefore taking high resolution TEM images in a short period of time requires a blessing. Obviously, this type of furnace-heating holder is good to perform low resolution in-situ TEM imaging [5–13]. As an application example, Fig. 3.2 shows a result of in-situ heating of a bilayer nanowire composed of a 20 nm-thick Cu layer and a 100 nm-thick SnO_2 layer. The bilayer nanowire was heated in a 300 kV transmission electron microscope. Because of the difference in thermal expansion coefficients between Cu and SnO_2, the bilayer nanowire curves toward the Cu side at room temperature as shown in Fig. 3.2a but becomes straight at 200 °C, Fig. 3.2b [9].

A demonstration of the in-situ wire-heating holder was reported by Kamino and Saka [14]. A spiral tungsten wire 20–50 mm in diameter is used to heat powder materials attached to the heating wire and is therefore based on a direct heating mechanism. The materials can be heated to as high as 1500 °C although the heating power is maintained at a low level, and the sample area being heated may be millions of times smaller than that of the furnace-heating holder. Cooling water is not required. The sample drifting rate due to the thermal expansion effect is tolerable ~10 min after temperature change, therefore atomic resolution at elevated temperatures is readily achievable as demonstrated in many published papers [14–23].

Figure 3.3 shows the kinematic growing process of a SiC crystal. Si particles on a graphite support were heated to 1500 °C in a 300 kV transmission electron microscope and the reaction between molten Si and graphite formed 6H-SiC.

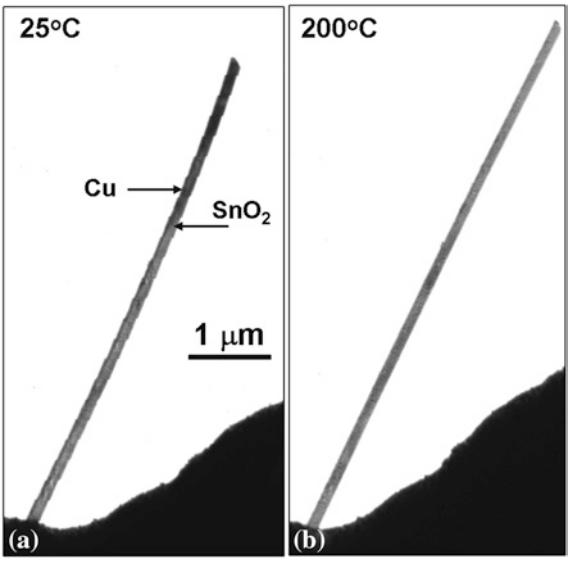

Fig. 3.2 TEM image of a 6.1 μm long bilayer nanowire composed of a 28 nm-thick Cu layer and a 90 nm-thick SnO_2 layer. The bilayer nanowire curves toward the Cu side at room temperature (**a**), and becomes straight at 200 °C (**b**)

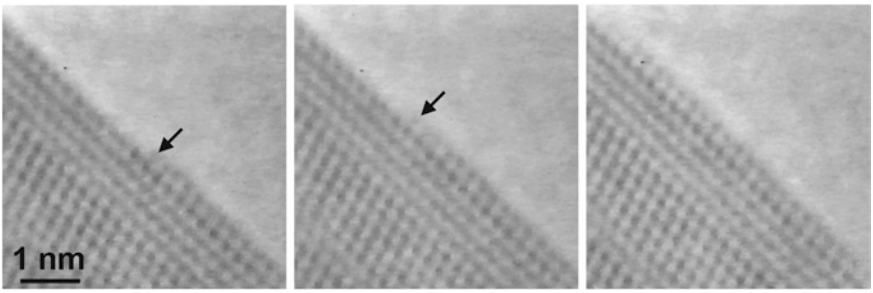

Fig. 3.3 In-situ TEM observation of SiC growth at 1500 °C. An atomic monolayer is seen growing on the SiC surface. *Arrows* indicate the very forefront atoms at the moment

The three images present the successive moments in growth of an atomic layer on the SiC surface [15].

Using the same concept, heating holders with two wire heaters [16], three wire heaters [18], and multiple wire heaters with a gas spray nozzle [24] were also developed for doing in-situ evaporation deposition in electron microscopes. Figure 3.4 is an illustration of a double-heater holder. Precursor materials on the upper heater can be evaporated and deposited onto the substrate mounted on the lower heater. Solid-liquid-gas interactions can thus be studied.

The membrane-heating holder is rather new compared to the furnace-heating and wire-heating TEM holders. The key component of this type of holder is a heating

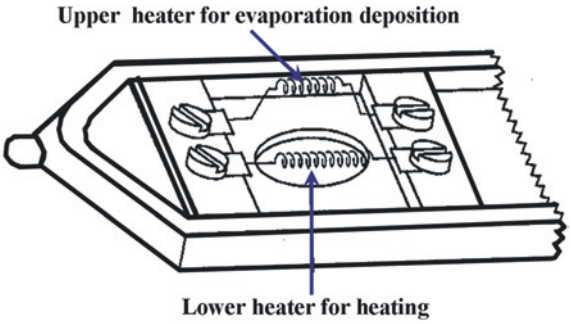

Fig. 3.4 Illustration of a double-heater in-situ TEM holder. The upper heater is for in-situ TEM evaporation deposition of materials onto a substrate positioned on the lower heater (Patent of Hitachi High Technologies Corporation, Japan)

device made from a conductive ceramic membrane suspended on a Si chip. Heating is very local and the heating power is small, resulting in a small sample drift rate at elevated temperatures. A very unique feature of the membrane-heating holder is the fast temperature change rate, as high as 10^6 °C/s is possible. This unique feature makes the holder a good choice for doing in-situ TEM thermal cycling experiments [25].

In addition to the three typical types of heating holders introduced above, a novel technology to be proven in applications is the in-situ environmental laser heating holder. The holder is assembled by a set of laser focusing and reflection optics. The laser beam heats a specimen without the presence of any heating elements. Temperature can be raised to beyond 2000 °C. The spot size of the laser beam and the irradiation position on the specimen can be varied. It is expected that the laser beam irradiation leads to a uniform concentric thermal expansion in the specimen, therefore minimizing uneven thermal stresses and ultimately a very low specimen drift rate is possible [26].

3.3.1.1 Chemical Analysis at Elevated Temperatures

Chemical analysis complements structural characterization is important for the in-situ heating TEM study because chemical processes are likely to occur when materials are heated. Energy-dispersive X-ray spectroscopy (EDS) and electron energy-loss spectroscopy (EELS) are two popular analytical methods associated with TEM. Because the EELS spectrometer is attached at the bottom of the electron microscope, its working condition is not influenced by field change in the microscope specimen chamber and is therefore ideal for in-situ heating TEM experiments. Kamino et al. demonstrated EELS analysis for SiO_2 at 700 °C [27]. In contrast, the EDS detector comes very close to TEM specimen (a few millimeters in distance), the infrared radiation from the heating zone may affect the detector, resulting in a dark current which in turn increases the noise in the X-ray signal detector. EDS analysis at elevated temperatures, e.g., 550 °C, was indeed reported [12]. At even higher temperatures, significant noise deteriorates the EDS energy resolution.

Figure 3.5 shows EDS spectra of a Si specimen in-situ heated in a transmission electron microscope equipped with a 30 mm^2 Si(Li) EDS detector. The full width

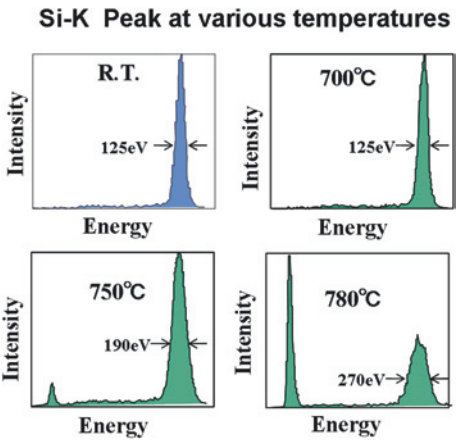

Fig. 3.5 EDS spectra showing Si-K peaks at room temperature and elevated temperatures. Deteriorated energy resolution is seen at 750 °C and above

at half maximum (FWHM) point of the Si peaks is marked for the peak acquired at room temperature, 700, 750, and 780 °C, respectively. It can be seen that the FWHM value remains unchanged untill 700 °C, but broadens at 750 and 780 °C. This test indicated a regular EDS performance until about 700 °C (for Si) but the energy resolution deterioration was prominent at higher temperatures. Covering the collimator of the EDS detector with a Beryllium window would solve this problem at the expense of detection sensitivity for light elements. Another concern is that the window in front of the EDS detector would become brittle if it is very close to the heating zone, and the cycles between room and high temperatures may eventually damage the window material and glue. The advice is, if the EDS detector is to be used in any in-situ heating TEM experiments, to consult with the EDS system provider beforehand.

The opposite of the in-situ heating TEM is cryo TEM using liquid nitrogen- (<100 K) or liquid helium- (4.2 K) cooled TEM holders. Although there were experimental examples for in-situ cooling TEM to reveal materials' responses to the low temperatures such as magnetic flux and vortices in superconductors at below 10 K [28], cryo holders are actually widely used for stabilizing the structure, reducing sample contamination rate and beam damage rate, and maintaining the temperatures required by frozen-hydrated biological samples (cells, tissues, macromolecules, viruses). The latest applications are in cryo electron tomography for three-dimensional imaging [29–31].

3.3.2 In-situ Gas Environmental TEM (ETEM)

From the engineering point of view, thermal and cryo fields are fairly easy to be introduced into the specimen area in the transmission electron microscope because the instrumental modification is limited to the TEM specimen holders. However, in our real world, many physical and chemical processes take place in an environment

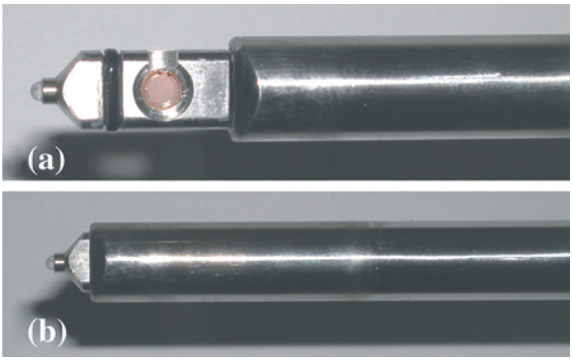

Fig. 3.6 An environmental transfer holder. **a** The specimen cup is in the Out position for specimen treatment in a reaction chamber outside of an electron microscope. **b** The specimen cup can be retracted and sealed in the rod of the holder to prevent air exposure during transferring from the external reaction chamber into the electron microscope column

filled with gas and/or liquid. For example, a catalytic process includes catalysts, gas, and a suitable temperature, which is, in most cases, higher than room temperature. It is clearly desirable to have an in-situ TEM technology that is capable of handling gas or liquid in the specimen chamber of the electron microscope.

As a simple and low cost solution, an environmental transfer TEM specimen holder may be a good compromise to partly meet the ETEM demand. Figure 3.6 shows a picture of such a holder. The tip of the holder where the TEM specimen locates is movable, so it can be retracted into the holder rod and sealed by an O-ring.

One can load a specimen into the holder, study the original state in an electron microscope, and then move the holder (with the specimen) to a reaction chamber outside the microscope. The specimen is treated in the reaction chamber under desired environmental conditions (gases, pressure, temperature, etc.). Before taking the holder out of the reaction chamber, the tip of the holder is retracted into the rod so that the specimen will not be exposed to air when transferred back into the electron microscope. The post-treatment structure can thus be studied. This type of transfer holder allows for a comparison between the material structures before and after material treatment but the middle links are unknown. An example is shown below.

Polycrystalline SiC was synthesized by hot pressing in the presence of aluminum, boron, and carbon additives [8]. About 1 nm-thick amorphous intergranular films were formed among SiC grains. After heat treatment at above 1000 °C for 3 days or more, the amorphous intergranular films seemed to disappear because the boundaries looked amorphous-free. In order to figure out where the amorphous intergranular films went, in-situ heating TEM was carried out. The grain boundary film with an amorphous structure shown in Fig. 3.7a was heated and monitored in a transmission electron microscope. The heating temperature was 1200 °C at which the sample was held for 25 h with the electron beam turned off to minimize the electron beam irradiation effects. Figure 3.7b shows the result. In fact, the grain boundary film remains at the same location but has been partially crystallized to form an Al-O-C structure.

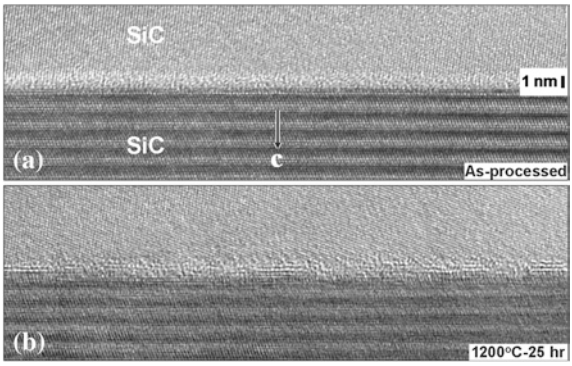

Fig. 3.7 **a** High resolution TEM image showing a 1 nm-thick amorphous intergranular film between two SiC grains. **b** After heat treatment at 1200 °C for 25 h in a transmission electron microscope, crystallized segments are observed along the intergranular film

The in-situ TEM observation clarifies the newly formed Al-O-C crystalline structure contained in the "clean" boundary. The structure is hard to distinguish from the SiC matrix because it is similar to the SiC structure and has an epitaxial structural relationship with the SiC (0001) surface.

There is no doubt that real in-situ ETEM is needed in many TEM characterization analyses, but accommodation of gas or liquid in an electron microscope column is by no means easy. An environmental cell (E-cell) in the microscope column is a key to confine the gas or liquid to the specimen area while the high vacuum level in the remaining parts of the microscope column should not be affected. There are two major types of E-cells: window-type E-cell and differentially pumped E-cell [32]. Designs are totally different and each has advantages and disadvantages.

3.3.2.1 Windows-Type Gas E-Cell

The window-type E-cell concept has a long history back to 1935. Shortly after the invention of the transmission electron microscope, a gaseous environment was introduced through the window-type E-cell to analyze hydrated biological samples and to investigate the contamination rate of the microscope column when using E-cells [32–34]. The so-called window-type E-cell is built in a TEM specimen holder at the tip area, Fig. 3.8. The TEM specimen sits inside the cell, which is then sealed by two windows above and below the specimen. The window materials must be electron transparent and have a weak interference with the electron beam. This means that the window materials should be amorphous in structure and thin enough. The window membranes must also be strong enough to withstand the pressure difference between the gas cell and the TEM vacuum. Typical window materials are amorphous carbon or silicon nitride with a 15–200 nm thickness depending on the desired gas pressure for the applications. The reported maximum gas pressure is 1 atmosphere while TEM imaging and electron diffraction could be done through a 15 nm-thick silicon nitride membrane window E-cell in a 300 kV transmission electron microscope [35]. The cell can be either standalone or with gas inlet and outlet ports.

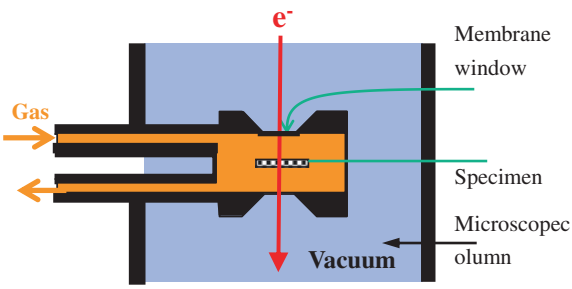

Fig. 3.8 Scheme of a window-type gas-flow E-cell in an electron microscope column. Gas is contained inside the cell without leaking into the microscope column

The biggest advantage of the window-type E-cell is the relatively low cost and microscope choice flexibility. Because the E-cell is built into the TEM specimen holder, no modification of the electron microscope is involved (microscope modification is expensive especially when the vacuum system is included) and the holders associated with any electron microscopes can be modified into the E-cell holders. High gas pressure is practical when choosing a robust window design. However, significant disadvantages prevented the window-type E-cell to become popular so far. First of all, it is tedious to assemble an E-cell, and the translation of specimen into the E-cell is not easy, if not impossible. As a consequence, sample exchange is a time consuming challenge. The searchable area on the TEM sample is quite limited. Second, electron scattering from the window materials and the high gas pressure (if applicable) interferes with electron diffraction, deteriorating image quality and resolution. For example, more than 90 % of the electrons at a 300 kV accelerating voltage are lost after penetrating through two 15 nm-thick silicon nitride window membranes and a 1 mm-thick air layer at 1 atmosphere gas pressure. Increasing the accelerating voltage helps to improve image quality, which was why ultrahigh voltage (million volts) transmission electron microscopes were pursued in 1970s for the window-type E-cell applications [32, 36]. However, expensive instruments, high maintenance costs, and high-energy electron beam-caused radiation problems eventually raised serious concerns. The request for ultrahigh voltage environmental transmission electron microscopes went down sharply in 1980s. Third, windows of E-cells may easily get contaminated as a result of deposition of materials evaporated from the specimen by the incident electron beam. Lastly, it is highly risky to heat materials to high temperatures because the window materials may crack, causing gas leakage. It should be noted that progress has been reported recently, where a window-type gas E-cell with a built-in thin wire heater demonstrated a 0.3 nm lattice resolution at 600 °C in a 10^4 Pa pressure environment [35].

3.3.2.2 Differentially Pumped Gas E-Cell

Limited by the obvious disadvantages of the window-type E-cells, attempts were made to leak gas into the microscope specimen chamber directly. In 1965, L.F. Allard and W.C. Biglow explored the possibility by finding out that a vacuum level of ~10^{-2} Pa was tolerable in the column of a transmission electron microscope

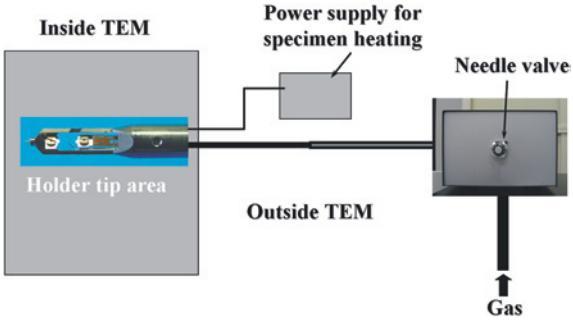

Fig. 3.9 Schematic illustration of working principle for a gas injection-heating holder. A heater heats specimen while a gas nozzle sprays gas directly onto specimen inside a transmission electron microscope (Patent of Hitachi High Technologies Corporation, Japan)

in their lab at the University of Michigan. They then managed to leak air into the microscope column to degrade the vacuum from 4×10^{-3} Pa to 7×10^{-2} Pa while a home-built TEM heating stage was used to heat a single crystalline Cu specimen. Real-time observation of the oxidation process was recorded via a 16-mm cine camera system.

A better method was reported in 1971 by Swann and Tighe [37–39]. An E-cell was built inside a transmission electron microscope, called a differentially pumped E-cell. This was a concept reported by Ruska in 1942 [3]. In this type of design, a significant modification of the electron microscope pumping system is needed. Gas can be injected into the specimen chamber directly either through a port on the pole piece [41–44] or through a specimen holder with a gas injection port and pipeline [27]. Figure 3.9 shows a picture of a gas injection-heating holder reported by Kamino et al. A gas nozzle is placed about 1 mm away from a wire-heating filament. With this design, gas can be sprayed directly onto a TEM specimen under heating [27]. In order to confine the gas within the microscope specimen chamber, a pair of gas restriction apertures should be added along the microscope column above and below the specimen position, Fig. 3.10. Typical bore diameters of these apertures are 0.1–0.3 mm depending on aperture positions. The apertures allow the electron beam to pass through for TEM observation but restrict gas leak from the specimen chamber to the rest of the microscope column. Although small gas leak is still inevitable, the leaked gas is pumped out by the turbo molecular pumps or molecular drag pumps between the restriction apertures [40–47].

The advantages of the differentially pumped E-cell are obvious over the shortages of the window-type E-cells. Because of non-existing window membranes above and below the specimen, the specimen is directly exposed to the electron beam, facilitating high-resolution TEM. For the same reason, heating the specimen to high temperatures is safe and specimen translation is not an issue. The constant gas flux also helps to reduce contamination build-up on the specimen. An apparent disadvantage is the increased cost for microscope construction because of the significant modification of the electron microscope columns. The restriction apertures below the specimen also limit high angle diffraction electrons to be recorded (not good for dark-field imaging). In addition, the maximum gas pressure in a

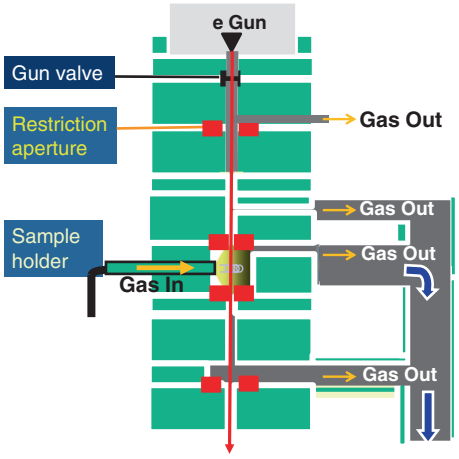

Fig. 3.10 Schematic illustration of a differentially pumped gas E-cell, which is a built-in part of an environmental transmission electron microscope. Gas is inlet into the specimen chamber and the restriction apertures *above* and *below* the specimen chamber reduce the gas leaking from the specimen chamber to the rest of the microscope column. Extra pumps are necessary to evacuate the gas leaked to *upper* and *lower column*

differentially pumped E-cell is limited to below 10^4 Pa in order to maintain the necessary vacuum level in other parts of the electron microscope column. In particular, electron microscopes powered by field emission guns typically require a vacuum of 10^{-8} to 10^{-9} Pa in the gun area, and such a high vacuum is difficult to maintain if the gas pressure is high in the differentially pumped E-cell chamber. In this sense, a LaB_6 electron emitter is better because it works in a vacuum level 3 to 4 orders of magnitude lower than that for a field emitter. The LaB_6 gun transmission electron microscopes have other advantages in the in-situ TEM applications. As the delocalization imaging artifact known from atomic resolution images is much less, therefore, atoms at the sample edges or grain boundaries can be clearly imaged. The high beam intensity of LaB_6 emitters is also ideal for high resolution in-situ TEM imaging. Needless to say, a LaB_6 transmission electron microscope is more affordable in terms of costs of purchasing and maintenance. With the technology advancement, affordable differentially pumped E-cell transmission electron microscopes with LaB_6 emitters became available recently [24, 27, 46].

In-situ gas ETEM has been widely applied to study structural evolution, phase transformation, shape dynamics, crystal or nanocrystal growth, catalysis processes, and oxidation/reduction behaviors [24, 27, 41–45, 48–54]. In addition, catalytic polymerization [55] and gas effect on dislocations [40] were also reported. Figure 3.11 shows an example of Si oxidation studied in a 300 kV transmission electron microscope with a differentially pumped system and a gas injection-heating holder [27]. The as-synthesized Si has a 3 nm-thick amorphous silicon oxide layer on the surface, Fig. 3.11a. The sample was first heated to 700 °C in a vacuum of 3×10^{-5} Pa. An electron beam of ~20 A/cm^2 beam current density was used for real-time, high resolution imaging during heating. The combination of the increased temperature and the focused beam irradiation knocked off the amorphous surface layer as shown in Fig. 3.11b. While the temperature was maintained at 700 °C, air was slowly sprayed onto the Si sample and the pressure

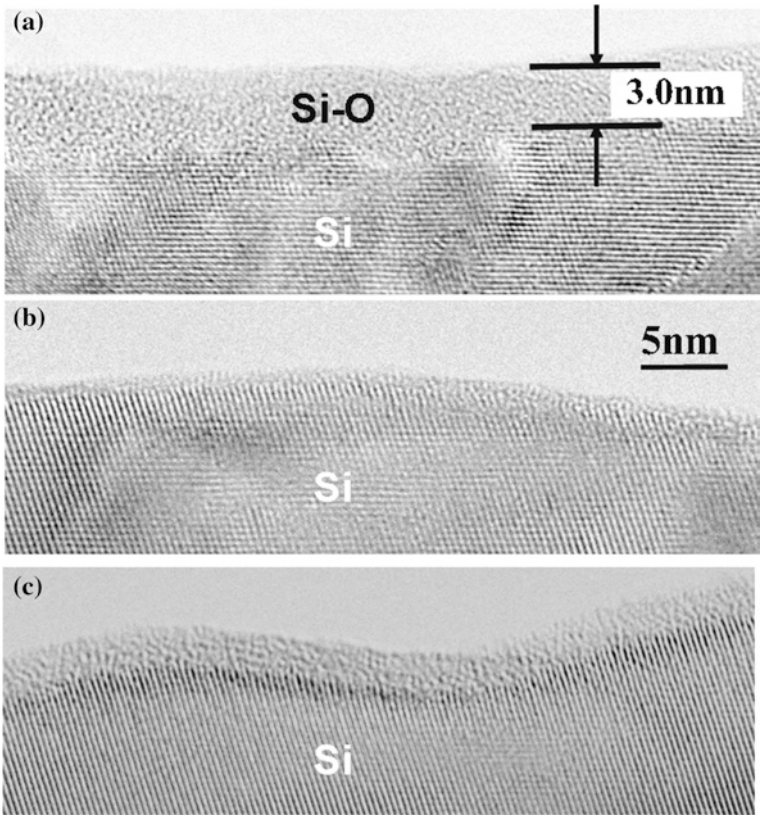

Fig. 3.11 In-situ TEM observation of Si oxidation at 700 °C. **a** As-prepared Si sample with a 3 nm-thick amorphous silicon oxide layer on the surface. **b** Heating the Si sample to 700 °C in a 300 kV H-9500 transmission electron microscope to burn off the surface oxide layer using high electron beam intensity. **c** Re-oxidation of the Si surface in an air pressure of 8×10^{-3} Pa at 700 °C

in the specimen chamber was increased to 8×10^{-3} Pa. Re-oxidation of the Si surface was observed and a 2 nm-thick amorphous surface layer was formed after about one hour as shown in Fig. 3.11c. EELS analysis confirmed the Si and O composition in the newly formed surface layer.

One last thing to address is the gas source used for in-situ gas ETEM. Typical gases used in the study of catalysts and nanomaterials include air [24, 27, 48], O_2, H_2 [40, 42, 49], N_2 [41, 49], He, C_2H_2 [56], C_3H_6 [55], Si_2H_6 [51, 54], Ge_2H_6 [52], and water vapor [43]. The easiest gas source is air, which can be leaked into the TEM specimen area through a built-in pipeline in a specimen holder [27] or a gas port on the pole piece of an electron microscope [40–42]. Home-made gas supply systems are usually simple and affordable, containing a couple of gas bottles and a gas mixture buffer tank. A needle valve or similar is often used to control the gas injection flow rate and consequently the gas pressure in the

microscope specimen chamber. If quantitative gas supply is required, the gas supply system needs to be more elegant. It generally contains 4 to 5 types of gases and a water bubbler (to provide water-saturated gases). The gas supply systems containing more than 10 types of gases are rare but exist. For quantitative gas mixture and delivery, high precision gas pressure gauges, mass spectrometers or gas chromatographs should be used. Computer-controlled commercial gas handling systems are available nowadays. Safety is most important, the gases in use should not cause damage to microscope components or injury to users. The room must be ventilated adequately all the time during the use of gas supply.

3.3.2.3 Spherical Aberration (Cs)-Corrected Gas ETEM

In the early years, the window-type E-cell was popular, and a wide pole piece gap was required to accommodate the thick E-cells. The thickness of the E-cell and the wide pole piece gap required ultrahigh voltage transmission electron microscopes (1 MV or higher) to deliver a powerful enough beam able to penetrate and to achieve sufficient image resolution. With the faded ultrahigh voltage microscopes and the advent of the Cs corrector for high resolution TEM [57, 58], the most attractive idea is to build the intermediate voltage (200 or 300 kV) environmental electron microscopes with aberration correctors. The aberration corrector helps to achieve an atomic resolution (0.1–0.2 nm) with a fairly large pole piece gap like 5–10 mm. With the progress in developing combined spherical and chromatic aberration correctors, atomic resolution should be possible to achieve even with a 10–20 mm wide pole piece gap. Such a wide pole piece gap will provide space for insertion of multi irradiation sources or manipulators to the microscope specimen chamber area.

An example of the Cs-corrected gas E-cell transmission electron microscope is the one installed in Brookhaven National Laboratory (USA) in 2007. A built-in differentially pumped system can hold a gas pressure up to 20 mbar (2000 Pa) in the specimen chamber. The pole piece gap is 5.6 mm and a 0.78 Å point-to-point resolution is attainable when gas injection is not in use. The cost for such a microscope is about 5–6 millions US dollars, and therefore is not something affordable by most research organizations. In addition to the high cost, the accessories used on such microscopes often considerably compromise the microscope performance because the aberration-corrected electron microscope is highly sensitive to its working environment. The deteriorated resolution may be due to manipulation controllers, power supply units, cables, the gas supply system, and extra pumps supporting the gas E-cells. More data are required to justify the merit of the very expensive aberration-corrected environmental electron microscopes.

3.3.3 In-situ Liquid ETEM

Both the window-type gas E-cell and the differentially pumped gas E-cell introduced in Sect. 3.2 can be modified to accommodate liquids.

3.3.3.1 Window-Type Liquid E-Cell

Marton was probably the first one to open the field of window-type liquid E-cell [33]. As early as 1935, he attempted to use two 0.5 mm-thick aluminum foils as windows to make liquid E-cells. Abrams and McBain in 1944 [59, 60] used plastic film windows less than 100 nm in thickness, and since then many window-type liquid cells adopted windows made from plastic films, coated with one or more additional layers of evaporated material like silicon monoxide, silicon dioxide, silver, or gold. Reviews for the designs and operation of E-cells in the early years can be found in [32, 36, 61–64].

One of the pioneers for applying the state-of-the-art liquid E-cell TEM in advanced materials science is an IBM group led by F. *Ross*. She and collaborators designed a window-type liquid E-cell TEM specimen holder to study electroplating processes at a nanoscale. In their liquid cell design, two Si wafers were used as the main frame. A $100 \times 100\ \mu m^2$ window was cut out in the middle of each wafer and covered with an 80 nm-thick SiN membrane. The membranes were thin and transparent to electrons so the electron beam accelerated by a 300 kV TEM could penetrate through. On one Si wafer, a 0.5–1 μm-thick SiO_2 spacer was patterned, a sealed compartment was therefore formed between the two Si wafers when glued together by epoxy. Liquid reservoirs were built to supply liquid electrolyte to the liquid cell and electrodes were made inside and out of the liquid cell. Using such a liquid cell TEM holder, ~5 nm resolution was achieved on an H-9000NAR 300 kV LaB_6 emitter transmission electron microscope. Ross and her colleagues studied the electroplating process of Cu on gold electrodes, the relationship between Cu nucleation rate and electric current density, the diffusion-limited deposition and stripping of Cu, as well as the preferred nucleation sites were discussed [65].

Following exactly the same concept but changing materials and component dimensions, H. Zheng and her colleagues probed the growth kinetics of Pt nanocrystals [66]. The liquid cell they used contained a 200 nm-high liquid compartment filled with 100 nanoliter precursor solution (Pt reagents and surfactants). In a short time intensive illumination under a 300 kV electron beam (LaB_6 emitter), Pt nucleation and growth were triggered. In the recorded streaming video files, mechanisms for Pt nucleation were discovered. Nuclei could grow either by adsorbing monomers from solution or merge with others to evolve into larger single crystalline nanocrystals. Regardless of the growth mechanisms, all of the Pt nanocrystals ended up with a similar shape and size after a certain period of growth time. The same method was then applied to study the real-time growth of Pt_3Fe nanorods at an atomic resolution [67], and to investigate the detailed structural evolution process that happened when the iron oxide nanoparticles in solution approached and attached to each other [68].

Although most high-resolution in-situ applications of the liquid E-cell reported in recent years were based on TEM observations, there exists a chromatic aberration effect for TEM imaging through thick liquid cells. Two approaches can be made to improve the imaging quality at the fixed electron beam energy: one

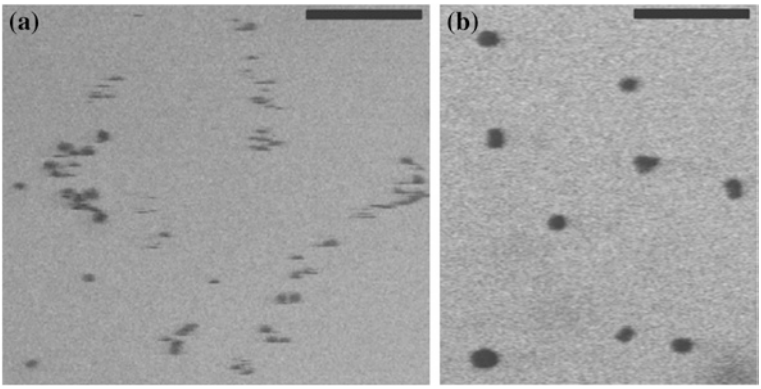

Fig. 3.12 STEM images of gold nanoparticles in water using a liquid E-cell holder. **a** 2–5 nm-diameter gold nanoparticles in water. The observed streaking was caused by particle movement under the influence of the scanning electron beam. **b** 10–20 nm-diameter gold nanoparticles in water. The scale bars correspond to 100 nm (Courtesy of Dr. James Evans, University of California at Davis, and Hummingbird Scientific)

is to make liquid cells and window membranes thinner and also minimize the liquid amount to a level just enough for wetting specimens. The single carbon atomic layer graphene was found to be a perfect support material to encapsulate a liquid solution for high resolution liquid TEM because of its high shape flexibility, mechanical tensile strength, and impermeability to small molecules. In combination with aberration corrected TEM, true atomic resolution was achieved in observation of the growth behavior of colloidal Pt nanocrystals in solution, the motion of as small as 0.1 nm radius Pt nanoparticles could be tracked [69].

Another approach is to consider alternative imaging modes, for example scanning transmission electron microscopy (STEM). Compared with TEM, STEM imaging is less affected by chromatic aberration due to the fact of no lenses below the specimen in the STEM ray diagram. de Jonge et al. achieved a better than 4 nm resolution in the STEM images for liquid materials [70, 71]. In their work, the liquid cell design was similar to the IBM version [65] except flowing liquid in the liquid compartment was enabled. Biological whole cells were grown directly on Si-N membrane windows and labeled with gold nanoparticles. The gold nanoparticles dispersed in the liquid were used to measure the STEM imaging resolution and the result was consistent to the theoretical calculation. In another example, Au nanoparticles with 2–5 nm and 10–20 nm in diameter, respectively, were imaged using a sealed, micro fabricated fluidic cell holder, Fig. 3.12.

It seems not impossible to obtain a better than 1 nm STEM resolution for imaging materials in liquid, but achieving much higher than 1 nm STEM imaging resolution may be obstructed by Brownian motion in liquid.

Strictly speaking, there is also the third way to get around the considerable chromatic aberration problem caused by the window-type liquid E-cell. The method is to accommodate liquid around the specimen without using the window-type liquid cells.

3.3.3.2 Liquid ETEM with an In-Column Differentially Pumped Liquid E-Cell

Several types of differentially pumped liquid E-cells were developed since 1968 in order to carry out electron microscopy studies on live cells and get electron diffraction patterns from wet biological crystals and wet cell membranes [72, 73]. The big advantages of accommodating liquids directly in electron microscopes are again the high resolution and lowered chromatic aberration effect because the total sample thickness is reduced. Gai et al. developed a TEM specimen holder to inject microliter liquid into the electron microscope specimen chamber and the specimen could be heated to elevated temperatures [74]. Using this holder on a modified 200 kV transmission electron microscope with a differentially pumped system, heterogeneous hydrogenation of polymerization in the presence of liquid, catalysts, hydrogen gas, and a thermal field were studied.

Another intriguing discovery that may lead to a progress in accurate delivery of small quantities of liquid into the local area on a TEM sample was reported by Sutter and Sutter [75]. In this work, a pipette made from a Ge nanowire as a body and an Au-Ge reservoir wrapped by a carbon shell as a liquid source were demonstrated. When heating to higher than 361 °C (eucentric temperature of bulk Au-Ge alloy), the Au-Ge alloy melted but was confined within the carbon shell. Once a fine hole was pierced into the carbon shell using a focused electron beam in a 300 kV transmission electron microscope, the liquid leaked out and formed dispensed liquid drops 20–40 nm in diameter.

3.3.4 In-situ Biasing TEM

In-situ biasing TEM, by its definition, means TEM observation of a specimen on which a bias voltage is applied. For electrical conductive specimens, a circuit can be formed with a TEM specimen as a component for electric current to pass through. In-situ biasing TEM is often used to study behaviors and structural changes of specimens in an electrical field, as well as electrical transport properties of individual nanostructures and Joule heating effects in microscale and nanoscale structures. Probe TEM specimen holders are popular for these application purposes. A built-in metallic probe with a tip of 50–100 nm in diameter can move back and forth in fine steps controlled by a piezo manipulator, so that gentle approach and contact is possible between the probe and the nanostructures. The probe is connected to a power supply unit by which a voltage can be applied to the specimen, which is at grounding potential. The probe can also be used to manipulate nanomaterials. All these are carried out with simultaneous TEM observations.

Using a probe TEM holder, a single-walled carbon nanotube of 12 nm in diameter and 24 nm in length was stretched in a transmission electron microscope to study the plasticity [76]. A constant bias of 2.3 V was applied and the Joule heating caused

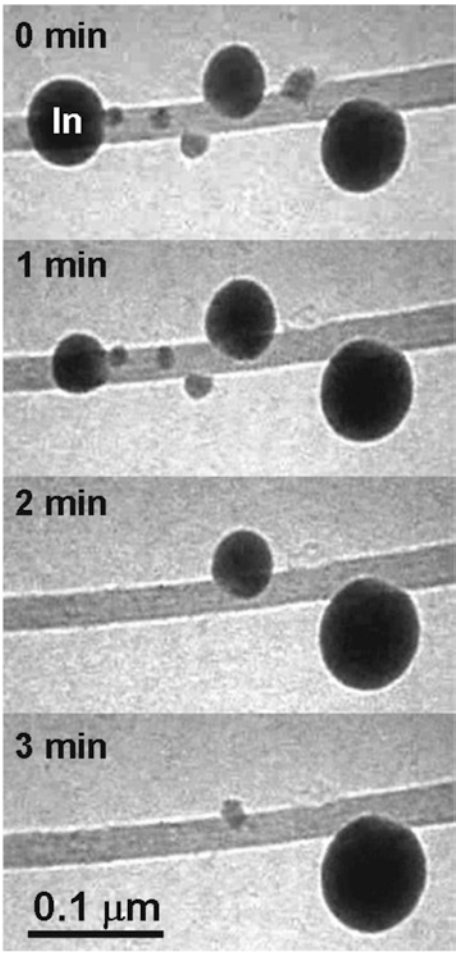

Fig. 3.13 Four TEM images, spaced by 1-min time increments, showing indium transport on a multi-walled carbon nanotube. The tip closer to the anode which is out of view to the *left* has a higher temperature than the tip to the cathode (out of view to the *right*). The mass transport is driven by the temperature gradient (Courtesy of Zettl Research Group, Lawrence Berkeley National Laboratory and University of California at Berkeley)

a temperature rise to about 2000 °C in the carbon nanotube. A 280 % tensile strain with a 15-fold reduction in diameter seen in TEM images revealed the superplasticity of this nanotube although a possible role of electron beam irradiation effect was not addressed. Using the same in-situ biasing TEM holder and experimental parameters, exceptional plasticity of double-walled and triple-walled carbon nanotubes (190 % elongation and 90 % diameter reduction) [77], and amorphous-to-crystalline structural transformation of carbon nanowires were also reported [78].

In another excellent example, nanoscale mass transport along carbon nanotubes was realized [79], Fig. 3.13. First, indium metal was evaporated onto multi-walled carbon nanotubes, which formed nanoparticles attached to the walls. Using a probe TEM holder, electric current was driven through the carbon nanotubes and the Joule heating raised the local temperature, resulting in a temperature gradient along the longitudinal axis of the nanotubes. When the local temperature was

above the melting point of the indium particles, atomic scale mass transport of indium to cooler zone was observed. The mass transport was reversible when the direction of the current flow was opposite [79].

Using the same principle, nanoscale cargos that not only translated along but rotated around a multi-walled carbon nanotube were observed using in-situ scanning electron microscopy (SEM) [80]. Although not mentioned clearly, the fabrication of the co-axial carbon nanotubes and application in the nanoscale cargo transport and rotation experiments was similar to earlier results reported by Cumings et al., in which a probe TEM holder with four electrical leads was used to open the tip of a multi-walled carbon nanotube and to peel off the tube wall layers [81] or pull the inner tubes out of the outer shells [82], Fig. 3.14.

A bias voltage of 2.9 V generated a 200 mA electric current through the multi-walled carbon nanotube and burned off the enclosed tip. Some outer tube walls were peeled away so the remaining tip became much sharper. The successive peeling and sharpening dynamic process were observed in a high-resolution transmission electron microscope [81]. The authors further demonstrated that the exposed inner tubes could be pulled out of the outer walls and then pushed back using the probe as a manipulator [82]. The TEM images and corresponding schematic representation in Fig. 3.14 clearly show the inner tubes sliding out and in, similar to an old style telescope. The result indicated an ultralow friction between each concentric tube walls and the multi-walled carbon nanotubes hold a great promise for nanomechanical applications because of the low-friction and the low wear nanobearing property [82].

As noticed a couple of times already, Joule heating is often an important part of the experiments using an in-situ probe TEM holder (e.g. Fig. 3.13). It can of course also be used for in-situ heating TEM observations. For example, electrically driven redox processes in cerium oxide films were studied. Ordered oxygen vacancies could be generated in CeO_2 thin films by passing an electric current (6 V) through the films. The films were oxidized again in the microscope chamber when the current was turned off [83].

For in-situ electrical transport measurements in transmission electron microscopes, the key is to make an ohmic contact between the nanostructure and electrodes provided by the in-situ probe TEM holder. In a successful attempt, conductance of an individual carbon nanotube was measured using a probe TEM holder, which was correlated to the structural changes imaged simultaneously [84]. In this work, a carbon nanotube with one end fixed to a conductive probe manipulator was pushed into a liquid metal (Hg or Ga) to make Ohmic contacts between the liquid metal and the suspending ends of the nanotubes. Two-point current-voltage (I-V) measurements were done while doing in-situ TEM observation. A ballistic transport feature at room temperature was revealed [85]. It was also demonstrated in other in-situ biasing TEM experiments that structural deformation plays an important role in the electrical conductance of carbon nanotubes [85, 86]. Similarly, electrical resistivity of ZnO nanowires was found to be linearly proportional to the bending degree [87].

In addition to the properties of individual nanotubes or nanowires, interconnections among nanostructures are also of great interest. Various shapes

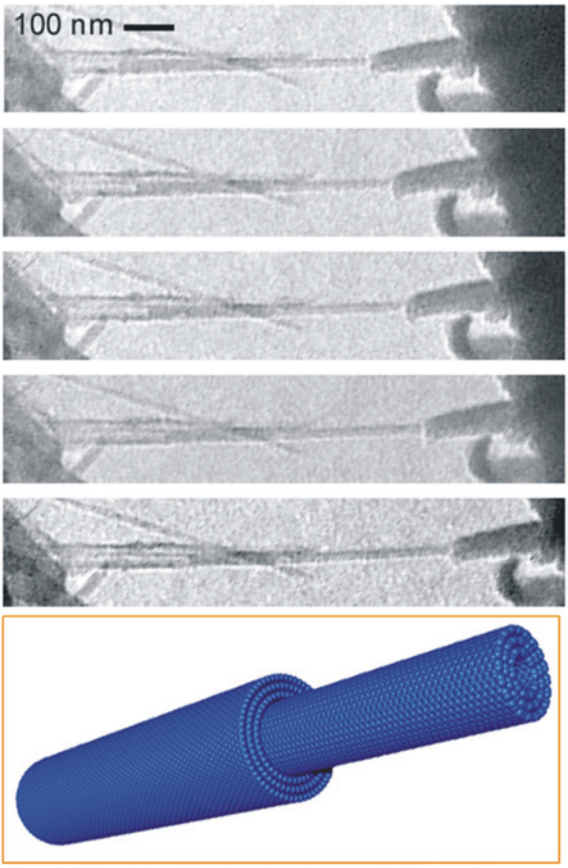

Fig. 3.14 A series of TEM images showing telescoping of a multi-walled carbon nanotube using an in-situ probe TEM holder. The model at the *bottom* illustrates the sliding of the inner tubes with respect to the outer shells as observed experimentally (Courtesy of Dr. John Cumings, University of Maryland)

of connections between carbon nanotubes were successfully fabricated taking advantages of a precise positioning control (0.02 nm) and in-situ soldering by electron beam-induced amorphous carbon or Joule heating-induced tungsten melting soldering. I-V curves of the tube/tube connections were measured and the junction resistance was lowered by graphitization of amorphous carbon bonding material [85–88]. Tips of carbon nanotubes were also modified in a transmission electron microscope and the I-V measurements clearly demonstrated the importance of the tip structure to the field emission characteristics [88]. The electric field not only triggered a field emission from the tips of carbon nanotubes, but was also used to field evaporate carbon nanotubes segment by segment, and the electron beam was intentionally used to adjust the field evaporation rate in a nanoscale area to modify the tip morphology [89].

In-situ biasing TEM is certainly useful in the study of nanoscale films and electronic devices. Local electrical transport properties in nanoscale magnetic tunnel junction thin films [90] and the effects of annealing on electrical transport of magnetic tunnel junctions [91] were investigated. In particular, tunneling

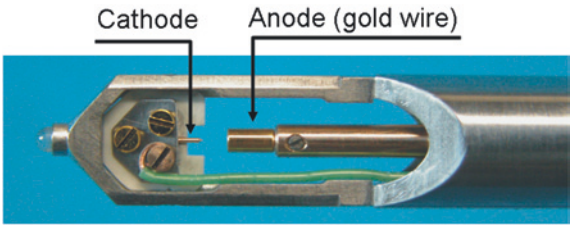

Fig. 3.15 A picture of the tip area of a dedicated electrode TEM holder. Voltages of up to 1 kV can be applied to the specimen (Patent of Hitachi Materials Research Lab, Hitachi Ltd)

magnetoresistance (TMR) of individual nanomagnetic tunnel junctions under working conditions were measured using the in-situ probe TEM holder [92]. Because the nanomagnetic devices were very small (100 × 150 nm^2 in area), in-situ TEM observation was essentially the only way to make sure that the piezo controlled probe could make a correct contact on the single device to be measured.

With great attention paid to the energy-related materials and processes in recent years, in-situ biasing TEM was recently employed to study the real-time charge-discharge process in nanomaterials-based lithium-ion batteries. Huang et al. built a nanoscale electrochemical device in an in-situ probe TEM holder and successfully observed the structural and morphological changes of the SnO_2 nanowire anode during the lithiation process. The SnO_2 single crystalline nanowire was converted to a Li_2O amorphous nanowire containing embedded Sn and Li_xSn nanoparticles and the process resulted in more than 200 % volume dilation [93].

Compared with the in-situ probe TEM holders, the dedicated electrode TEM holder has a simpler design as shown in Fig. 3.15 but a much higher voltage can be applied.

Anode (gold wire) and cathode are integrated into the tip of a TEM holder. The distance between anode and cathode can be adjusted from 0 to 5 mm, and voltages of up to 1 kV can be applied [94, 95]. The specimen to be studied is mounted on the cathode and the distance between the specimen and the anode is typically 0.5 mm. A voltage applied via the cathode causes a potential difference across the specimen. Such a holder has been used together with the in-situ Lorentz TEM to investigate the field emission of multi-walled carbon nanotubes [94, 95], and high voltages (800–900 V) were found particularly valuable in these studies [96]. Also, using a specially designed field-effect transistor-based biasing holder, chiral indices and chirality-dependent transport properties of double-walled carbon nanotubes have been studied [97].

3.3.5 In-situ Nanomechanical TEM

Mechanical properties such as strength, hardness, and toughness may be changed significantly when the sizes of materials go down to nanometer scales. With increasingly miniaturized electronic components and the request to correctly understand and predict failure of nanostructures, material size effects on mechanical

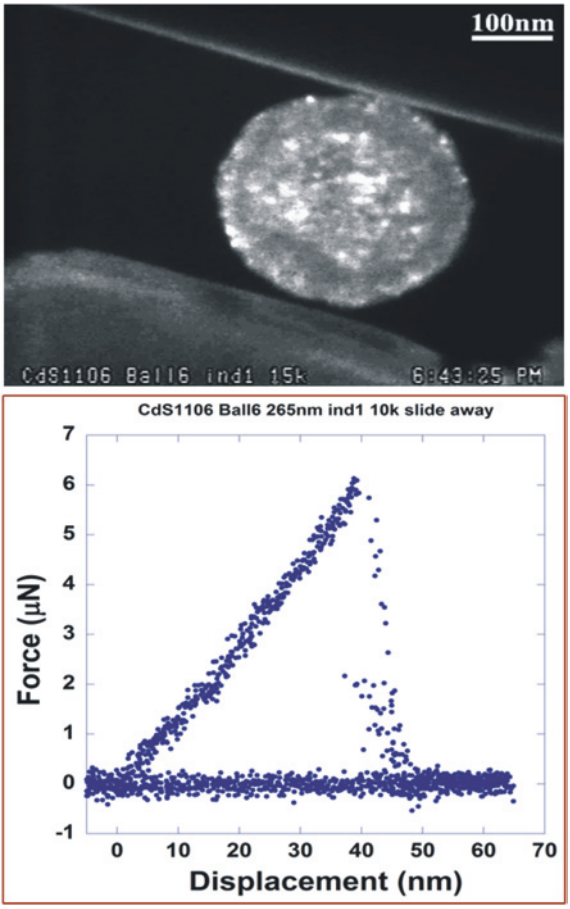

Fig. 3.16 TEM image of a CdS spherical nanoparticle under a compression force. The corresponding Displacement-Force curve acquisition and TEM observation were performed simultaneously in real time. The sudden load drop at about 6 mN was not due to a catastrophic failure but sliding of the nanoparticle away from the site as revealed by TEM observation (Courtesy of Dr. Zhiwei Shan of Hysitron Inc. and Dr. Andy Minor of Lawrence Berkeley National Laboratory)

behaviors become more important and urgent than before. Like all other in-situ TEM technologies, the development of in-situ nanomechanical TEM was because of the high resolution that TEM can offer for direct imaging and characterization of internal structures and defects in materials. A good example was given by Z.W. Shan et al. for why in-situ TEM is necessary for nanomechanical testing [98].

Figure 3.16 shows a CdS spherical nanoparticle under a constant compression force. The ball was gradually compressed and the corresponding Displacement-Force curve tells a linear relationship between force load and deformation displacement. The load drops suddenly at about 6 μN, which may imply a catastrophic failure of the ball. However, simultaneous TEM observation told a different story, the CdS nanoparticle did not break but slid away. This beautiful "seeing is believing" example again reminds a possibility of misinterpretation of experimental data if real-time in-situ TEM observation is not available.

In fact, in-situ experiments in the late 1960s and early 1970s already showed a capability for direct observation of mechanical indentation, compression, and

bending deformations in scanning electron microscopes and transmission electron microscopes [99, 100]. After decades of development, precisely controlled, quantitative in-situ nanomechanical TEM holders have been developed to characterize the mechanical behaviors and corresponding structural changes in micro and nanostructures [101]. One of the pioneering works on the in-situ nanomechanical TEM was to measure the elastic modulus of carbon nanotubes [102]. In this work, a custom-built TEM holder was used in which carbon nanotubes were attached to a gold wire through which an electric potential was applied to the nanotube. Static and dynamic mechanical deflections were induced in the multi-walled carbon nanotube cantilevers in a transmission electron microscope [102]. Although the elastic properties were successfully derived in the experiments, the method used is not easy to be expanded to nanomechanical testing of other nanostructures of various shapes. Obviously, specially designed straining TEM holders are required to load a tensile or compressive mechanical force on TEM specimens while tracking real-time structural changes in order to find out and quantify mechanical property-structure relationships. Various TEM holders with different designs have been reported, including conventional tensile straining holders, microelectromechanical systems (*MEMS)-based straining* holders, nanoindentation holders, and TEM grid-based straining holders.

3.3.5.1 Conventional Tensile Straining TEM Holder

The concept of the conventional straining holder for in-situ electron microscopy originated in the late 1960s [103–105]. The basic idea was to make a specimen in a rectangular shape with one end fixed and another end connected to a movable rod, which could slide along the length of the holder. Figure 3.17a shows a picture of such a holder (tip part) for in-situ tensile straining TEM. The letter p labels two pins, the pin to the left is connected to a sliding rod. The sample is made into an 11×3 mm rectangular shape as shown in Fig. 3.17b. The central area is thinned for TEM observation and the two holes on both sides of the thinned central area are used to positioning the sample along with the pins shown in (a). Clamps and screws are used to secure the sample into the holder tip. When pulling the sliding rod, a tensile straining force is applied to the central sample region where in-situ TEM observation is performed [106]. The sample shown on the right side of Fig. 3.17b is after in-situ straining TEM.

As an application example, Fig. 3.18 shows a real-time TEM observation of dislocation-precipitate interaction processes in a stainless steel sample under a tensile straining force. The dislocations pinned by carbide precipitates eventually bypassed the pinning sites via either a simple mechanism or a complex configuration [107]. In particular, roles of hydrogen in enhancing the mobility of the dislocations and in determining the cracking rate along certain directions were discovered using a tensile straining holder working with a gas E-cell [41, 107]. Using a similar specimen holder, dislocation dynamics, as well as fracture and plasticity deformation mechanisms in nanocrystalline nickel were studied comprehensively [108–110]. Heating or cooling is also possible for some straining TEM holders.

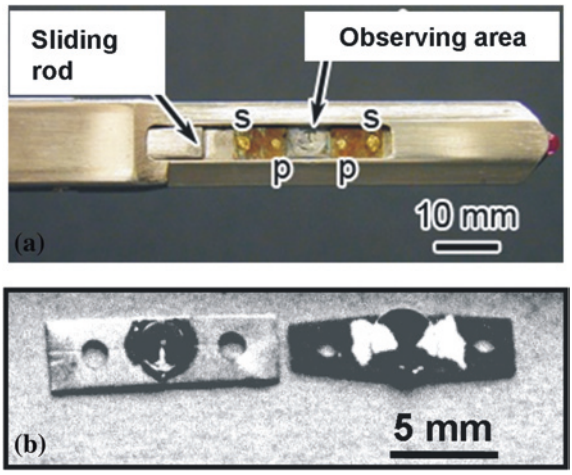

Fig. 3.17 **a** A picture for the tip area of a conventional tensile straining holder. **b** A specimen (*left side*) prepared for in-situ tensile straining TEM, two holes at the two ends are used to align the specimen with the two mounting pins on the holder (labeled *p* in **a**). The pin to the *left* in **a** is connected to a movable rod. Clamps are placed over the mounting pins and the specimen is further secured to the position via screws (labeled s in **a**). The specimen to the right in **b** is after a straining TEM experiment (Courtesy of Dr. Ian Robertson of University of Illinois at Urbana Champaign)

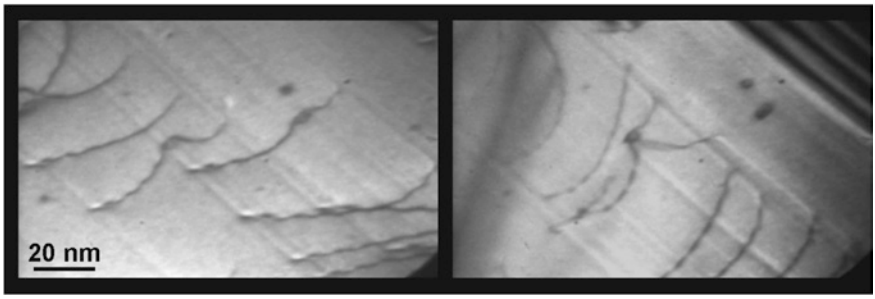

Fig. 3.18 In-situ TEM images showing dislocation-precipitate interactions in a stainless steel specimen at room temperature. The dislocations pinned by precipitates (*black dots*) could bypass the pinning sites either in a simpler way (*left*) or in a complex way (*right*) (Courtesy of Dr. Ian Robertson of University of Illinois at Urbana Champaign)

3.3.5.2 MEMS-Based Straining TEM Holder

A deficiency of the conventional tensile straining TEM holder described above is its inability to quantify the force load and material deformation displacement. In addition, only tensile force can be applied. To overcome these problems, MEMS-based mechanical testing holders were designed [106, 111]. The key part, a free-standing MEMS chip device integrated into the tip of the holder, is fabricated using the standard silicon-based microfabrication followed by lift-out from the substrate, Fig. 3.19.

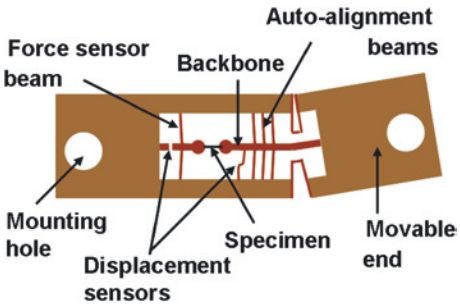

Fig. 3.19 Schematic illustration of a free-standing 10 mm × 3 mm MEMS chip device which can be integrated into the tip of a TEM holder for uni-axial tensile testing

The force load is applied with a displacement-controlled mechanical, thermal, or electrostatic mechanism and the applied load and straining are measureable by displacement-force sensors or differential capacitive sensors. Both tensile and compressive forces are possible to be applied. The dimension and shape of such a MEMS chip device is similar to those of the specimen shown in Fig. 3.17b. Using a MEMS device with thermal actuation and capacitive load sensing, in-situ mechanical testing and TEM observation were performed on multi-walled carbon nanotubes, whereby elastic modulus and fracture strength close to theoretical predictions were confirmed [112, 113]. Details in designs, working principles, experimental examples, and related references for various MEMS devices for in-situ nanomechanical TEM can be found in [111].

3.3.5.3 Nanoindentation TEM Holder

The development of nanoindentation TEM holders catalyzed quantitative in-situ compressive straining TEM studies. Loading rate control at micronewtons/s and displacement rate control at nanometers/s are feasible now driven by mechanical/piezo positioning elements or nanoscale positioning motors. A flat-tip of the nanoindentation holder is made from diamond or tungsten, which is used to punch into a specimen. As can be seen in Fig. 3.20, the indentation is from a side direction, while the electron beam coming from top, images morphological and structural changes in the deforming area. Specimen used with this type of nanoindentation holder are either thin films coated on substrates, nanomaterials attached to supporting subtracts, or crystals made into a pillar shape with a sub micrometer diameter. A focused ion beam (FIB) system is often required to fabricate micro pillars because FIB makes sample preparation site-specific and dimension/geometry-controllable. However, because FIB is Ga ion milling-based, it inevitably changes surface structure of materials and in turn has effects on mechanical testing results. The influence of ion beam milling is increasingly prominent with decreasing object size as a result of the larger surface to volume ratio. Caution is therefore called for data interpretation if specimens are prepared using FIB.

Various nanostructures have been studied using the in-situ nanoindentation TEM holders. A classic in-situ nanomechanical TEM work is shown in Fig. 3.21.

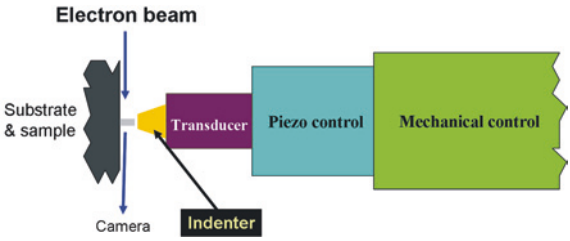

Fig. 3.20 Schematic illustration of a nanoindentation holder for in-situ nanomechanical TEM (Courtesy of Dr. Zhiwei Shan and Dr. Oden Warren of Hysitron Inc.)

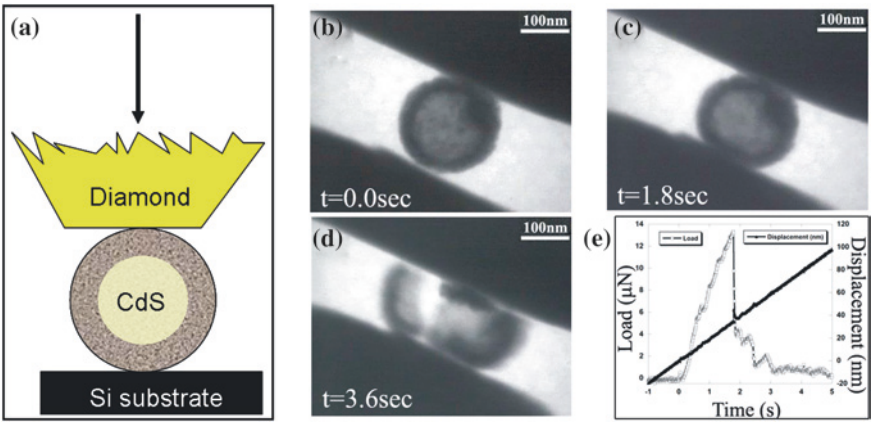

Fig. 3.21 In-situ nanomechanical TEM result obtained using a nanoindentation TEM holder. The specimen was a hollowed CdS nanoparticle. **a** Scheme of the indenting area. For the simultaneous TEM observation, electron beam is parallel to the paper-normal direction. **b–d** A series of TEM images showing morphological changes of the nanoparticle from beginning (no load) to failure at the time of 3.6 s. **e** Time-Load-Displacement curves recorded simultaneously with TEM observation (Courtesy of Dr. Zhiwei Shan of Hysitron Inc.)

A nanocrystalline CdS hollowed sphere with a diameter of 210 nm was applied a compression force in a transmission electron microscope. The compression rate was 20 nm/s and Time-Load-Displacement curves were recorded in real-time accompanied by the correlated shape change revealed by time-resolved TEM imaging [114]. Figure 3.21a shows the beginning state and Fig. 3.21b corresponds to the peak load of 13.2 μN right before fracture is observed in Fig. 3.21c. An effective stress of 370 MPa, a compressive strain of 16.4 %, and a stiffness of 2.3 GPa were derived. The values indicated that the stress in the nanocrystalline hollow sphere was quite large although the effective stiffness was much smaller than in the bulk counterpart [114].

In-situ TEM mechanical testing of WS_2 nanotubes was reported using a holder with a sharp W tip as the indenter and a flat Pt tip as a support to WS_2 nanotubes. Both W and Pt tips also served as electrodes to pass electric current through the nanowires [115].

In-situ nanomechanical TEM on sub-micrometer diameter, FIB-prepared, pillar samples has a great advantage in probing the size effect, e.g., uni-axial size-dependent strength. Experiments showed a surprising "mechanical annealing" effect in which defects in single crystalline Ni pillars, 150–400 nm in diameter, could be completely removed simply by applying a mechanical stress [114]. Using the pillar samples, systematic in-situ TEM investigations of size effects were also performed on single crystalline Ti-Al alloy pillars with diameters between 8 and 0.4 μm. 1 μm diameter was found to be a mechanism transition threshold below which the compression deformation mechanism changed from deformation twinning to dislocation plasticity. The maximum flow stress saturated at a value close to the ideal strength of bulk Ti [116].

3.3.5.4 TEM Grid-Based Straining Holder

Recently, an innovative method was developed to conduct in-situ tensile and bending of nanowires in a transmission electron microscope [117–122]. An epoxy with desired strength was used to make colloidal thin films (polymer with high strength and transparency) supported by commercially available 3 mm-diameter TEM grids. The thin films were intentionally broken prior to or during TEM observation. Figure 3.22a is a schematic illustration of a Cu grid covered with a colloidal thin film on which nanowires were randomly scattered. In a transmission electron microscope, the colloidal thin film was heated or irradiated by electron beam to make it curling or shrinking. Both mechanisms usually started from the broken edges as shown in Fig. 3.22b and c. As a result, some nanowires on the film were wrapped into the curled thin films, they were either bent [120, 121] or under an axial tensile force [117–119].

Figure 3.23 shows in-situ TEM images of an amorphous silica nanowire. A uniform and dramatically reduced wire diameter accompanied by axial elongation indicates a super-plastic mechanical property of this specific nanowire [119]. The initial nanowire diameter is 36 nm, which decreases to 20.3 nm after tensile deformation. The deformation spreads across a rather wide region (~700 nm, marked by the two white bars in Fig. 3.23h) without obvious necking (an indicator of quick glass break). This tensile experiment indicated a super-plasticity of about 215 % for the silica nanowire studied.

Using the same method, in-situ tensile straining TEM investigations were performed on Si nanowires [117], and SiC nanowires [118]. Figure 3.24 shows a case of bending a Si nanowire. The bending was imaged in real time imaged at low and high magnifications. The high-resolution TEM images show full dislocation activities (c and d) [121]. Distinctive features of the incipient elastic-to-plastic transitions between the tensile and compressive regions of the bent nanowire are clearly seen. Burgers vectors of the dislocations are determined from the high-resolution TEM images (c and d) [121]. Bending of SiC nanowires was also investigated, elastic deformation, elastic-to-plastic transition, and plastic deformation processes were successfully captured at nanoscale and atomic scale in a transmission electron microscope [122, 123].

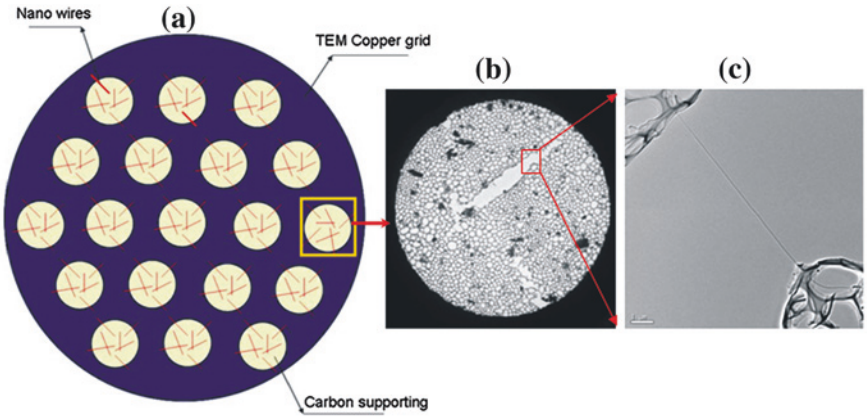

Fig. 3.22 The colloidal thin film contraction method for generating a tension force on nanowires. **a** A drawing of a TEM Cu grid. **b** TEM micrograph for a hole on a TEM grid covered with a carbon supporting film. **c** Pulling of a single nanowire by the contracted carbon film (Courtesy of Dr. Xiaodong Han and Dr. Ze Zhang of Beijing University of Technology, China)

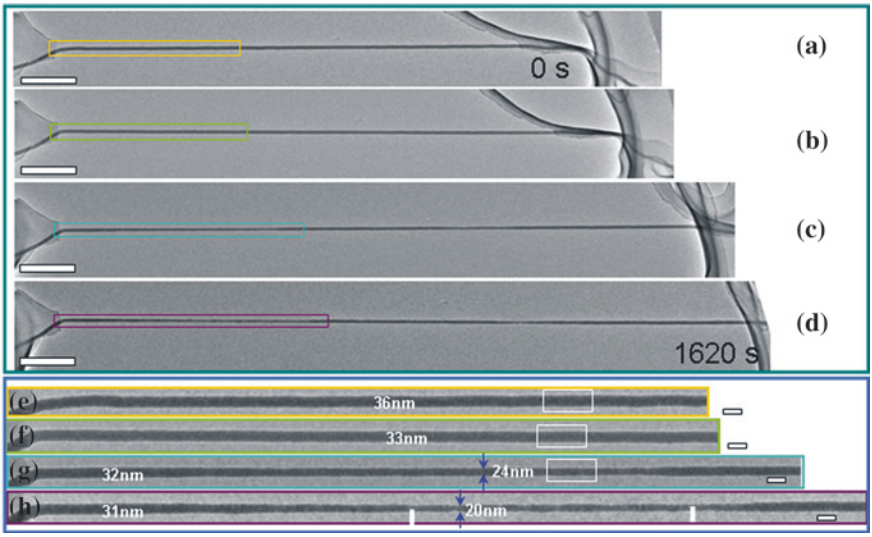

Fig. 3.23 In-situ TEM images showing a superplastic elongation of a silica nanowire under a tensile force and a moderate electron beam illumination. **a**–**d** The large strains, with the framed areas magnified in **e**–**h**. Scale bars **a**–**d** 500 nm, **e**–**h** 50 nm (Courtesy of Dr. Xiaodong Han and Dr. Ze Zhang of Beijing University of Technology, China)

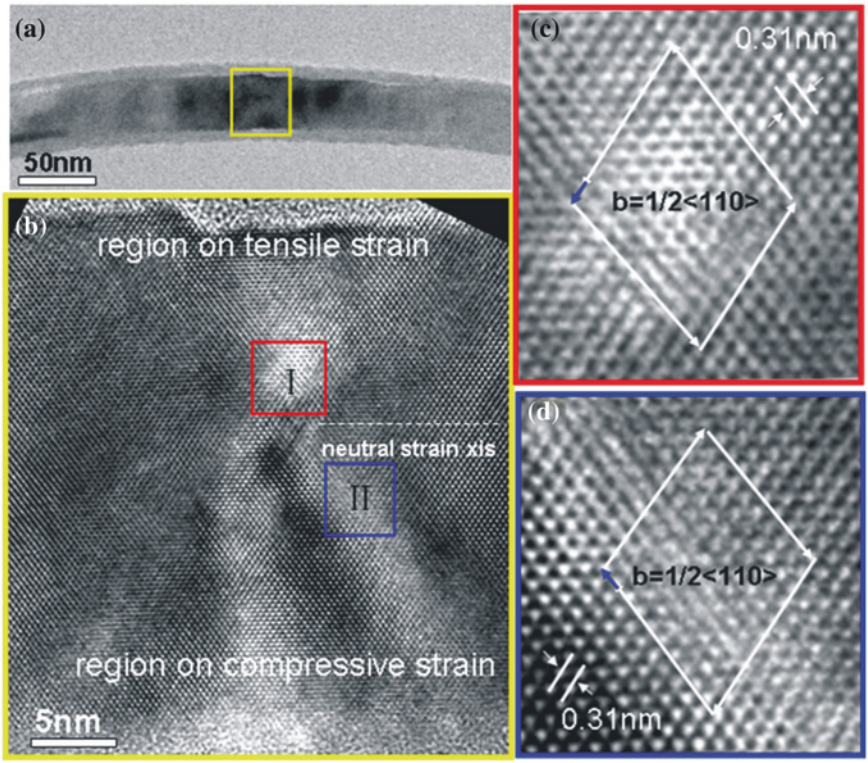

Fig. 3.24 A bent Si nanowire. **a** A low magnification TEM image. **b** A high resolution TEM image taken from the framed region in **a**. **c** and **d** show high resolution TEM images of the framed regions *I* and *II* in **b**, respectively (Courtesy of Dr. Xiaodong Han and Dr. Ze Zhang of Beijing University of Technology, China)

This section about in-situ nanomechanical TEM focuses on typical instruments, methodologies, and material systems. Nevertheless, nanomechanical property testing is not limited by the aforementioned in-situ nanomechanical TEM holders or methods. For example, it was reported that multi-walled carbon nanotubes could be turned into a pressure cell to study the effects of high pressure on nanomaterials [124]. In this example, carbon nanotubes filled with Fe_3C, Fe, or Co were heated to 600 °C in a 300 kV field emission transmission electron microscope. The purpose of the heating was to mobilize defects in the graphite structure of the carbon nanotubes so to prevent defect agglomeration, which might destroy the nanotube structures rapidly. Self-compression of the carbon nanotubes induced by electron beam irradiation generated a compression force on encapsulated nanomaterials. ~40 GPa pressure or higher pressure deformed, extruded, and broke hard materials such as Fe_3C as clearly confirmed in the in-situ TEM experiments [124]. Because of the page limit of this chapter, some other areas such as in-situ TEM nanotribology and in-situ mechanical testing on biological materials are not covered.

3.3.6 In-situ Lorentz TEM and In-situ Electron Holography for Imaging Magnetic or Electric Field Distribution

For TEM imaging of the materials containing magnetic or electric field, two TEM techniques are commonly used, Lorentz TEM and electron holography.

3.3.6.1 Lorentz TEM: Principle

This is a phase contrast TEM imaging technique, which is used to observe magnetic domains. It is based on a phase shift in incident electron waves caused by magnetic specimens. Two imaging modes are routinely used. Fresnel mode (under- or over-focus imaging) is used for imaging magnetic domain walls. It is also sensitive to the change of electrostatic potential in specimens. Foucault mode (similar to dark-field imaging) is mainly used to image magnetic domains [125].

In the Fresnel mode, defocus leaves alternating bright and dark lines in a TEM image, the bright lines occur at the position of magnetic domain walls at which the magnetizations on both sides deflect the electrons towards the wall. If a coherent electron source is used, the convergent image of a magnetic domain wall is composed of a set of electron diffraction fringes running parallel to the wall. The over-focus imaging condition causes an image contrast reversal, see example in [126]. To image magnetic domains using the Foucault mode (dark-field-like), the objective lens of transmission electron microscope is kept in-focus, an electron diffraction pattern is first obtained in which diffraction spots split due to the magnetic field in materials. One of the diffraction spot in the split spot pairs is chosen to pass the objective aperture to form microscopy images.

The advantage of the Lorentz microscopy is to directly observe important features such as location and direction of the magnetic domain walls over a large field of view (up to tens of microns) and almost any modern transmission electron microscopes can do the job. The shortage is that the specimen surrounding area in the electromagnetic objective lens must have negligible external magnetic field strength. A popular solution to reduce the influence of the magnetic field coming from the objective lens of electron microscopes is to turn off the objective lens as well as the pre-field objective lens used for focusing the electron beam. The remnant magnetic field at the specimen location can be reduced to 200–300 Oe, which is, however, still influential for some soft magnetic materials. In addition, image focusing will have to be realized using the first intermediate lens and TEM magnification is limited to the use of the second intermediate lens and projector lenses. As a consequence, the magnification power is rather weak, usually lower than 10,000× [127].

The compromised Lorenz TEM performance on standard electron microscopes makes the dedicated Lorentz transmission electron microscope a better choice. The dedicated Lorentz microscope uses a weakly-excited long-focal length objective lens (on the order of more than 10 mm compared to ~2 mm for a standard lens) and the specimen is located above the pole piece gap where the magnetic

field is a few thousand times lower than that within the pole piece gap. Recently, a transmission electron microscope with dual specimen stages was invented with a quickly switchable conventional TEM mode and a dedicated Lorentz TEM mode [128–132] therefore the microscope can be used for both routine TEM characterization and for dedicated high resolution Lorentz TEM.

3.3.6.2 Electron Holography: Principle

For materials containing magnetic or electrostatic fields, the phase of incident electron waves are modified when the electron waves exit the TEM specimens. Recovering the phase of the exited electron waves will reveal the electric or magnetic information in specimens. Electron holography is a technology that measures both phase and amplitude of the electron waves. Two or more electron waves with different phases are brought into interference and form interference image (electron hologram), which contains three-dimensional amplitude and phase information at an atomic resolution level. In contrast, the phase information is not available from all other electron microscopy imaging techniques. Off-axis electron holography is the most widely used holography mode nowadays [133], in which an electron wave passes through a specimen (the objective wave) and a reference electron wave travels in vacuum. An electrostatic biprism system below the objective lens combines the objective wave with the reference wave, the interference between the two waves with different phases forms an electron hologram [134–136]. The phase difference stems from a phase shift occurred in the objective wave when passing through the specimen, and can be recovered to retrieve the magnetic or electrostatic potentials in materials. Recent advancement in multiple-biprism electron holography made this technology even more flexible and powerful [128–132, 137–139].

3.3.6.3 In-situ Lorentz TEM and In-situ Electron Holography

If in a TEM study the specimen is under a versatile environment such as temperature change [129, 140, 141], external magnetic field [142–145], bias voltage in active functional devices [146–152], or electric current [139, 153–155], one most likely should consider in-situ Lorentz TEM or in-situ electron holography. If an external magnetic field is required, in-situ TEM holders should be integrated with Helmholtz coils or electromagnets to generate a magnetic field at the TEM specimen area [143, 144, 156–159]. Another method to apply a magnetic field to the specimen inside a transmission electron microscope is to tilt the specimen in the intrinsic magnetic field of the objective lens [160–162]. It is also possible to bring a piezo-driven magnetic needle close to the specimen [163, 164]. The magnetic field in the specimen chamber of a transmission electron microscope can be measured using a modified TEM holder with a Hall sensor, Hall probe, or samples with known magnetic response together with magnetometers [165]

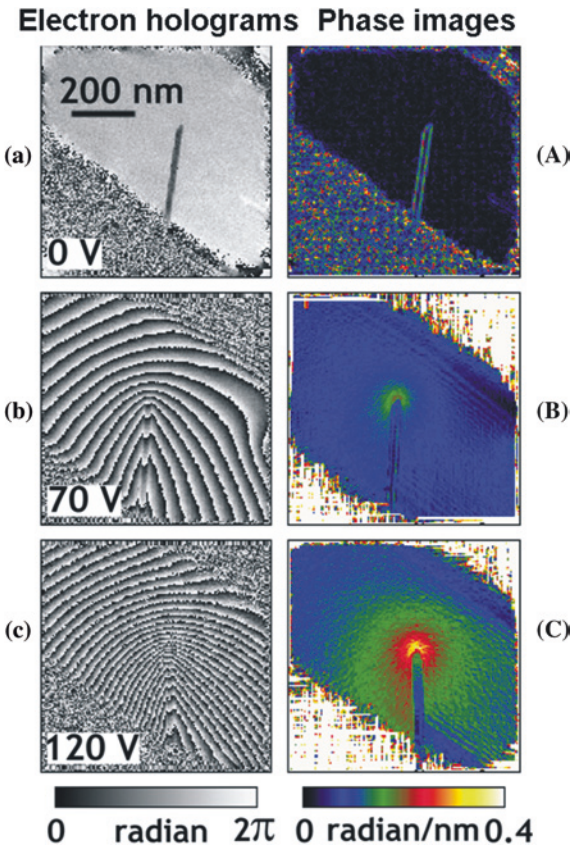

Fig. 3.25 Electron holograms (*a*)–(*c*), and corresponding electron wave phase images (*A*)–(*C*) for a carbon nanotube applied with a 0, 70, and 120 V bias voltage, respectively. In this field emission study, the phase images show the electric field distributions around the tip of the nanotube (Courtesy of Dr. John Cumings of University of Maryland)

As an example, in-situ electron holography was used to map the electric field distribution surrounding charged carbon nanotubes [166]. The experiments were special because the biprism used for electron holography was also made from a multi-walled carbon nanotube [167]. It was found that a 70 V electric field activated electron emission from the tip of a carbon nanotube. This field emission became stronger at 120 V. Electron holograms were recorded as shown in Fig. 3.25a–c, in which phase shifts of the electron wave at applied bias voltages of 0, 70, and 120 V were revealed as shown in Fig. 3.25a–c.

It can be seen that no electric field exists at the zero bias voltage. At 70 and 120 V bias voltages, high phase gradients, which correspond to electric potentials are seen at the tip of the carbon nanotube specimen. No high concentration of electric potential was seen at other locations along the nanotube length. The electric field strengths were derived based on a comparison between the experimental data and theoretical calculations. The measured data also concluded that for the same bias voltage, the local electric field strength at the tip of the nanotube was inversely proportional to the nanotube diameter [166].

Following the in-situ Lorentz TEM imaging principle, field emission of multi-walled carbon nanotubes were also studied using an in-situ biasing TEM holder (see Fig. 3.15) which allows a bias voltage of up to 1 kV and wide gap of up to 5 mm between the tip of a nanotube and the surface of anode. The wide gap, typically 0.5 mm in the field emission study, helps to avoid the electric discharge and the influence of outgas from the electrode. The large electric field induced high electron emission from the tips of the nanotube specimens and the observed emission current fluctuation at >20 mA was attributed to a peel-off damage of the carbon nanotubes as observed in TEM images [94, 95], and the liquid characteristic of Fe particles at the tips of carbon nanotubes was found to be related to the temperature effect due to the high emission current [96].

3.3.7 In-situ Ion Beam Irradiation TEM

All of the in-situ TEM technologies except in-situ ETEM introduced so far are on the basis of design or modification of TEM specimen holders. Differentially pumped E-cell needs the addition of gas restriction apertures and an extra pumping capability on the electron microscope column. There is another type of technology, in-situ ion irradiation TEM, which also requires extensive modifications on the microscope column. An ion beam is used to bombard the specimen while the effects are monitored in real time using TEM. The bombardment effects include phase changes and segregation, mechanical and structural changes, atomic mixing and chemical disorders, compositional changes, chemical reactions, grain growth/shrinkage, precipitation/dissolution, defect or bubble formation/growth/motion/coalescence/removal, destruction, ionization, diffusion, and collision cascades. Ion beam irradiation TEM became possible since 1961 [168] and has been well developed and applied for nuclear materials, space and astronautic engineering materials, semiconductor materials, materials for irradiation environments, ion implantation, and deformation mechanisms in materials.

More than 30 units of ion irradiation transmission electron microscopes were ever built in the world since 1961, and 11 of them were still in operation as of 2009 [169]. In most cases, one or two ion beam lines were introduced into the microscope column and guided to the specimen area for bombardment. Ion sources could be light or heavy ions such as H, He, O, Ne, Ar, Fe, Ga, Kr, Xe, or U, and beam energies range from a thousand volts to a few million volts. Usually one ion beam line is not so difficult to interface with an electron microscope at low elevation angles. Adding two or three ion beam lines, especially at high elevation angles requires complicated modifications on the electron microscope column, but the reward is the capability of using more than one irradiation condition to explore the combined effects.

There are many technical requirements for a transmission electron microscope to adopt ion beam lines while it maintains a sound TEM performance. First of all, ports are needed and must be vacuum-tight when connecting to ion beam lines.

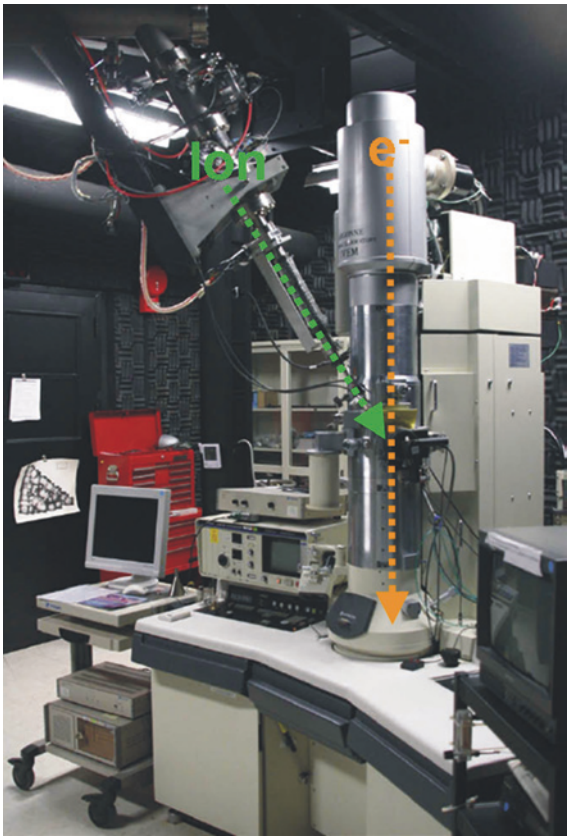

Fig. 3.26 300 kV H-9000NAR transmission electron microscope with an ion beam line introduced from a side direction as marked in the figure. The ion beam and electron beam hit the TEM specimen simultaneously. This microscope at Argonne National Laboratory is the only one of its kind in the USA

The pole piece gap should be wide enough to accommodate the beam lines and the associated accessories such as Faraday cups and electrical connections for measuring the ion flux arriving at the specimen. Both extra ports and a wider pole piece gap compromise the TEM imaging resolution. The resolution deterioration may be 30–50 % but atomic resolution should still be achievable in modern high-resolution transmission electron microscopes. The beam lines can target the specimen from high (as high as 90°) or low (as low as 0°) elevation angles but there are some TEM operation limits for the low angle ion beam lines [169]. Active and passive anti-vibration measures on electron microscopes and appropriate room designs are also important to minimize the excessive vibration caused by ion beam lines and ion sources.

One of the best known, active and productive ion irradiation TEM instrument is at Argonne National Laboratory, USA, Fig. 3.26.

It is usually fully occupied by many ongoing materials research projects. One of the applications was to use various heavy ions at different energies to bombard the $YBa_2Cu_3O_{7-d}$ superconductor single crystals to investigate irradiation damages at high resolution [170].

Another case in which a significant modification of the electron microscope is necessary is so-called the ultrafast TEM or dynamic TEM (DTEM). This is a technology that uses two synchronized laser beams with nanosecond or femtosecond pulses to generate electrons for TEM imaging and for inducing structural changes in the specimen. Details are introduced in Chap. 4 of this book and therefore will be skipped here.

3.4 Some Important Notes

3.4.1 In-situ TEM: Holders and Atomic Resolution

From the above introduction into in-situ TEM technologies, one should be able to make an important point: *To some extent,* in-situ *TEM is all about specimen holders.* External fields, forces, or exotic environments can be applied to a TEM specimen area through specially designed specimen holders. There is really not much technical limit to the holder-based in-situ TEM technology if one has great imagination and creativity. Exceptions do exist; they are chamber-based technologies like differentially pumped E-cell (Sect. 3.3.2.2) and ion beam TEM (Sect. 3.3.7).

Taking the most popular in-situ heating TEM as the first example, heating mechanisms vary for different advantages (Sect. 3.3.1). If more than just heating is desired, such as in-situ evaporation deposition, one may squeeze two or three heaters into the holder's specimen cup (Sect. 3.3.1). The second example is about site-specific in-situ heating TEM on interfaces or grain boundaries. Manual cross-sectional sample preparation is not only time consuming but also ends up with random chances of having the interesting, sub-micrometer structural features involved in the TEM observable area. A FIB system is known to be precise for lifting out a microscale piece of sample from the site-specific area (e.g. at an interface) and then thin it for cross-sectional TEM observation. A FIB/TEM compatible in-situ heating holder was thus developed to emphasize this advantage. Figure 3.27 shows pictures of such a holder used by Tanigagaki et al. [171]. At the holder tip, a tungsten heating filament is used for the in-situ heating purpose. The holder was first loaded into a FIB system for preparation of a microscale site-specific cross-sectional sample containing an interface between a Mo film and Ta substrate. A lift-out piece was mounted onto a heating filament and the knob at the holder handle was turned to the "FIB" position in order to thin the sample by a 40 kV Ga ion beam (Fig. 3.27a). Once the sample was thinned and ready for TEM observation, the holder was pulled out from the FIB system, the knob at the holder handle was turned to the "TEM" position and then the holder was loaded into a transmission electron microscope to do in-situ heating TEM study on the Mo/Ta interface [171].

Improving resolution has always been a major pursue on the roadmap of electron microscopy and instrument developments, and in-situ TEM has been following the same trend. Along with the efforts to bring various external fields or forces to the TEM specimen area, in-situ TEM at atomic resolution is never forgotten, although such a high resolution is not always feasible. Some key requirements must be met by both electron microscopes and specimen holders in order to achieve atomic resolution in-situ TEM.

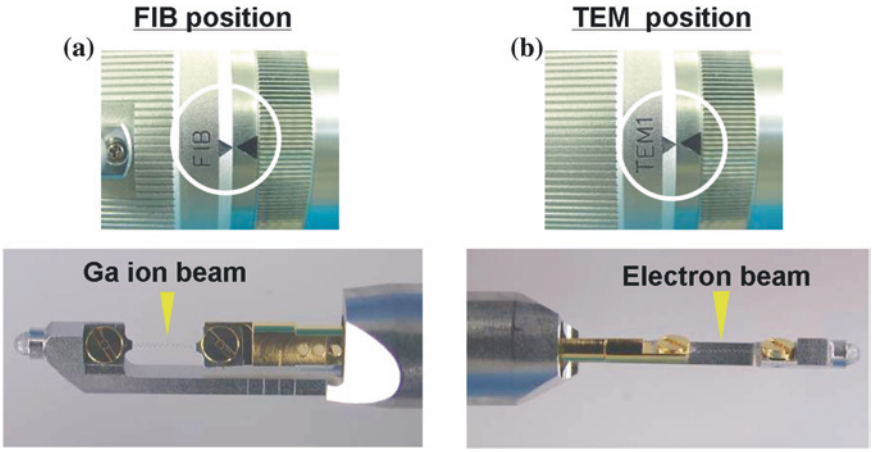

Fig. 3.27 In-situ FIB/TEM specimen holder allows preparation of a microscale site-specific cross-sectional TEM sample in a FIB system with the controller turned to position (**a**), the FIB position. After sample preparation by FIB, the controller of the holder is turned to position (**b**), the TEM position, and the same holder is then used to perform in-situ heating TEM (Patent of Hitachi High Technologies Corporation, Japan)

For the electron microscope, a large pole piece gap provides spacious room for inserting devices, illumination or field sources, or manipulators. However, the TEM image resolution will be compromised. For ETEM with gas injection ports on the pole piece, the electro-magnetic field within the pole piece may become asymmetric which lowers the image resolution, too. An optimized pole piece gap is crucial if atomic resolution in-situ TEM is a target. Additional pumps are often necessary for ETEM systems, therefore suitable anti-vibration system should be considered to reduce the vibration. Gas injection rate, total gas pressure or liquid amount surrounding a specimen should also be well controlled to minimize the influence on resolution.

For the in-situ TEM specimen holders, rule number 1 is simplicity. The design, arrangement of devices or field sources, sample fixation, wires, and pipelines should all be made or arranged in a way as simple as possible. For heating holders, it is extremely important to minimize or if possible eliminate the support grid, which usually contributes a major part of sample drift at temperature change. Keeping the power supply low and field- or force-application area local are proven to be efficient for lowering the sample drift.

3.4.2 Effects of Electron Beam Irradiation

As charged particles, electrons interact with matter much stronger than neutral X-rays or neutrons do. One of the often asked questions or discussed topics is the electron beam irradiation effects on phenomena observed during in-situ TEM

experiments. The question is natural because in-situ TEM experiments are different from routine TEM observation. in-situ TEM often concentrates on one specific area and the observation may easily take a few tens of minutes or hours. Also, in order to continuously record the structural evolution, electron beam intensity must be kept high enough to maintain suitable imaging conditions. Such a long time electron beam irradiation itself may introduce more considerable changes in the materials compared with normal TEM experiments. How to decouple the beam effects from applied field effects is always a challenge.

Electron beam irradiation effects are complex. Heating (energy transfer), ionization (radiolysis, breaking bond), knock-on or displacement (knock atoms out of their lattice sites), electrostatic charging (electron transfer), and sputtering (remove atoms from surfaces) are main damage mechanisms [172]. Ionization damage may cause severe problems for organic or oxide materials but less problematic for metallic or semiconductor materials frequently studied with in-situ TEM because the ionized electrons can be rapidly replaced. Electron beam heating effect often raises a question about the real temperature at the specimen, although the temperature in the specimen chamber can be derived or directly measured [48]. Depending on materials, beam current, thermal dissipation, and other factors, the rise in temperature in a TEM specimen may range from a few to more than a hundred degrees Celsius which sometimes is high enough to cause visible structural changes such as motion of dislocations and defects [173–176], or phase transformations at much lower than nominal temperatures [177]. For the liquid TEM, the interaction between the high energy electron beam and the chemical solution produces species and/or hydrated electrons which may play an important role in the observed nanocrystal growth or interaction behaviors.

To know how to reduce the electron beam damage to certain materials is nontrivial, because the damage mechanisms are usually interrelated and material dependent. One popular way is to adjust the accelerating voltage of the electron beam. Increasing voltage reduces the thermal and ionization damages but enhances the knock-on damage and the surface sputtering and vise versa. Depending on materials to study, one must choose an optimum accelerating voltage to minimize the combined beam damages. For example, using 40–60 kV accelerating voltage for imaging carbon materials (the knock-on displacement threshold for carbon is between 27 and 95 kV [178]), 74 kV or lower for BN nanotubes [179], and 200 kV or lower for Si can largely minimize the knock-on damage. In combination with the favorable beam energy, reducing as much as possible the beam current and shortening the beam illumination time should also be considered. Based on this consideration, electron microscope alignment and routine astigmatism correction should be done in an unimportant specimen area, and electron beam should be blocked when illumination is not absolutely necessary. Figure 3.28a shows a case of the knock-on damage by a 300 kV electron beam (15 A/cm^2) to an amorphous carbon shell surrounding a TiO_2 nanoparticle. The damage became significant after 10 min beam irradiation, therefore it was hard to study the graphitization of the amorphous carbon shell by in-situ heating TEM. To shorten the exposure time, the electron beam was blocked after taking an initial

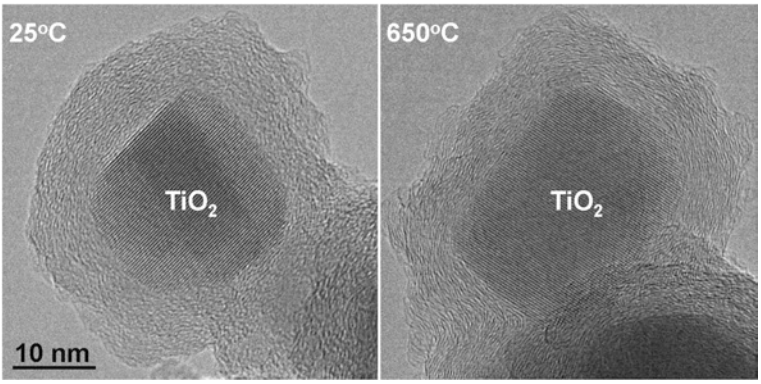

Fig. 3.28 A practical example of reducing electron beam irradiation effects in an in-situ TEM experiment. **a** As-prepared TiO_2 nanoparticle wrapped with an amorphous carbon shell. The image was taken at room temperature in a 300 kV H-9500 transmission electron microscope. **b** The specimen was heated to 650 °C and held for 20 min with the electron beam blocked, and then beam exposure was resumed for imaging. Total electron beam irradiation time was no longer than 5 min (the particles shown in two images are not the same ones.)

image at room temperature. The temperature was then raised to 600 °C using an in-situ heating TEM holder followed by resuming the electron beam illumination to image the structural change. It was clear that the carbon shell was graphitized by the thermal field (Fig. 3.28b) rather than electron beam irradiation.

Figure 3.7 shows a similar example, in which a SiC sample was heated for 25 h in a transmission electron microscope. Because the electron beam was shut off, the observed crystallization of the amorphous intergranular film was clearly independent of the electron beam effect.

Good conductive contacts between specimen and support or TEM holder also enhance thermal dissipation and reduce charging therefore minimizing the electron beam-induced temperature rise on the specimen and the charging effect. Cooling and beam shower (short time pre-illumination with a strong electron beam flux) help to retard or reduce the electron beam-induced sample damage and/or contamination process. Coating a layer of carbon on the sample surface may prevent sputtering damage. It was also reported that heating some specimens could heal the beam damages. Figure 3.29 shows a multi-walled carbon nanotube damaged by 200 kV electron beam (8 A/cm^2) irradiation for 20 min at room temperature. The corresponding EELS spectrum shows a broadened graphite σ* peak. Heating the sample to 600 °C largely decreased such beam damage as evidenced in the TEM image and the well-defined σ* peak in the corresponding EELS spectrum. It was actually a self-healing process in the damaged carbon regions.

Similar healing phenomena under irradiation of a 200 kV electron beam were found to cause superplasticity in amorphous SiO_2 nanowires and nanoparticles [119] and to improve the fracture strength of carbon nanotubes [112]. Heating may also cut down the hydrocarbon contamination rate by a factor of 10–30 depending on temperatures used [175].

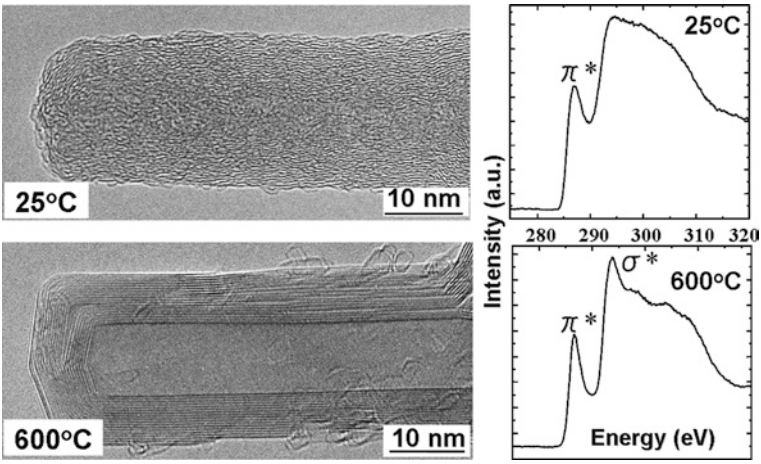

Fig. 3.29 Irradiation effects of a 200 kV electron beam on a multi-walled carbon nanotube. At room temperature, the electron beam deformed the graphite-like structure on the nanotube walls. EELS spectrum shows a broadened carbon σ* peak. Under the same electron irradiation condition, no distinguishable structural deformation on the nanotube walls was recognized at 600 °C, and EELS spectrum shows well-defined σ* peak (Hitachi High Technologies Corporation, Japan)

No matter what beam energy, electron imaging conditions, and other countermeasures are chosen, electron beam irradiation-induced damages to specimens can never go to zero especially after hours of in-situ TEM observations. In fact, it is often seen that the structural changes stem from a combined effect of the applied fields and the electron beam irradiation [119]. Caution is always needed in data interpretation. It should be a good habit to at least check the less or not irradiated neighboring specimen areas to make a comparison with the areas under an intensive and long-time electron beam illumination in order to understand and exclude the electron beam effects.

It is interesting to note that in some reported in-situ TEM experiments, electron beam irradiation effects were intentionally used to initiate dynamic processes. For example, electron beam irradiation was utilized to create knock-on displacement of carbon in multi-walled carbon nanotubes at 600 °C and the shrinkage of the carbon nanotubes resulted in a high pressure on the Fe_3C crystal(s) encapsulated inside the carbon nanotubes [124]. Similarly, carbon onions showed self-compression, too, under electron beam irradiation at ~700 °C [180]. Another experiment was about the role of electron beam irradiation on electric field evaporation of carbon nanotubes. The onset field for evaporation to start was lowered by about 30 % when the electron beam (200 kV, 100 A/cm^2 beam current density) was turned on, and the knock-on effect was believed to be the main reason [89]. Going back to Sect. 3.3.1, a 300 kV electron beam with a beam current density of 2–14 A/cm^2 transferred electrons to the Pt(acetylacetonate)$_2$ liquid solution and reduced Pt^{2+} to Pt [66]. Some beam effects are more significant with high gas pressure in gas ETEM. For example, gas molecules may be ionized by the electron beam, making

the molecules more reactive to interact or etch solid materials. The electron beam may also have a potential to be used as electron tweezers to manipulate defects in materials.

3.4.3 Digital Recording

A picture is worth a thousand words, a movie tells a story. The in-situ TEM is about discovering dynamic responses of materials to the externally applied stimuli. In most cases the responses include the structural evolution and many critical structural changes such as phase transformation or melting often take place suddenly without a clear clue beforehand. Therefore, knowing how, and having a live TEM observation capability is only the first step, recording what is seen at an adequate time resolution is equally important. The conventional film camera takes at least 10 s (including film transportation) to complete one exposure, this speed is orders of magnitude slower than that of TV cameras (30 frames/s), and certainly cannot satisfy the needs for instantaneous exposure and continuous high-speed image recording. Video recording for the entire in-situ TEM process is the best way to guarantee the capture of any critical moment and the continuous evolution processes in materials.

Before digital CCD (charge-coupled device) cameras became prevalent in TEM applications in the 1990s, analog TV systems were used starting in the 1980s. Electron microscopes output TV signals in standard video formats (NTSC: 525 lines/50 Hz, or PAL: 625 lines/60 Hz) which allowed users to view the live images on a TV screen and record videos using standard video cassette recorders (VCR). The standard frame rate was 29.97 frames/s, or 33 ms per frame. The large information capacity of the magnetic cassette tapes could support up to 10 h of video recording, reviewing the recorded movies was pretty easy. The problems were editing and analysis. The video file recorded on a magnetic tape needed to be converted to digital using a special and costly instrument in order to clip videos, grab single still frames and add texts or other necessary illustrations. Also, the recorded video frames were not quantitative in terms of image intensity linearity. Other problems for the TV cameras included uneven background noise, poor dynamic range (only ~10^2), a few tens of times smaller field of view than that of the TEM film cameras, and non-square pixels [181].

The 21st century is the digital century with no exception for cameras used for TEM. Digital CCD cameras are currently used on all state-of-the-art transmission electron microscopes, darkrooms for film development and image printing have become history in many laboratories. The high sensitivity, high dynamic range, high image intensity linearity, correctable background noise, and convenience for frame analysis and editing make the CCD cameras ideal for in-situ TEM. Via software, continuous digital image output from electron microscopes can be captured and made into movie files with the formats of avi, wmv, mpeg, etc. It should be noted that the video referred here is defined as a continuous

stream of images in time, therefore not necessarily to be NTSC or PAL format. A wide range of CCD recording frame rates are commercially available, and 10–30 frames/s are typically desired for the purpose of in-situ TEM. Higher frame rates are certainly desirable but the shortened exposure time for each frame lowers the image quality. The frame size in digital video recording varies but is typically in the range of 1024 pixel × 1024 pixel or smaller as of today yielding to the high speed.

The recent progress in developing CMOS (complementary metal oxide semiconductor) imaging sensors sheds a light on high speed and high sensitivity digital streaming video recording. Because no charge transfer will be necessary, each pixel on the detector chip takes and processes electrons simultaneously on their own, this is different from the working principle of the CCD cameras. Digital TEM cameras with a frame rate of 1000 frames/s will become a reality in the near future although there is still a concern about whether or not the number of electrons recorded on each frame is adequate to present images well. Another concern is that if computer processing and image saving speeds cannot keep pace with the frame capture rate, frames will be dropped from time to time resulting in sacrificed time resolution and information lost. With the advent of digital video recording technology, high computer processing speed and associated information technologies, such a frame drop problem is possible to be avoided. Large hard disk capacity is a must for the live digital video recording which easily generates 20 MB/s or more information to be saved, 500–1000 GB capacity should be available for each in-situ TEM experiment with a typical 2–4 h total time of video recording. Sometimes multiple hard disks are used to save image frames so that frame dropping will not happen.

3.4.4 Technical Challenges Ahead

In the past more than half century, in-situ TEM technology development mainly focused on developing capabilities of applying fields and/or environments to the specimen area while performing TEM observation. The attention now moves to pursue the atomic spatial resolution and high temporal resolution. High priority will also be given to quantitative in-situ TEM technologies in the near future. Although no one will argue that in-situ TEM is entering into a booming time, continuous and innovative efforts are required to conquer technical and engineering challenges that lie ahead, these include but are not limited to:

– How to precisely control and quantitatively measure the applied fields or exotic environments at TEM specimens, for example temperature, gas pressure, gas or liquid composition right on TEM specimens?
– How to enable the atomic resolution TEM imaging in versatile environments applied to TEM specimen chambers?

– How to achieve sub-nanometer or higher imaging resolution for the in-situ liquid E-cell TEM? Chromatic aberration-corrected TEM is certainly one of the solutions although the cost is high.
– How to squeeze multiple external fields or illumination sources into the narrow pole piece gap of a transmission electron microscope while maintain high resolution power? A large pole piece gap combined with aberration-corrected TEM is promising.
– How to observe, capture, and store high quality images at high temporal resolution on a level of microseconds to picoseconds? The pulsed laser beam-induced ultrafast TEM (see Chap. 4) may make a breakthrough in this aspect.
– How to analyze the recorded amount of digital data in a quantitative and efficient time?
– How to identify the side effects of electron beam irradiation and to reduce their influences?
– How to deal with beam-sensitive materials? This is a particularly tough challenge for in-situ TEM from the technical point of view.

3.5 Summary

Depending on what external fields or forces that are applied to the specimen in a transmission electron microscope, one can have in-situ heating TEM, in-situ cooling TEM (LN_2 and LHe), in-situ environmental TEM (gas or liquid), in-situ biasing TEM (electric voltage and current), in-situ straining TEM (tension or compression), in-situ Lorentz TEM, in-situ electron holography TEM, and in-situ ion beam (or laser) irradiation TEM available for study of materials in stimulating environments. Real-time in-situ TEM observations at high spatial and time resolutions for dynamic structural processes are becoming routine nowadays. In most cases, the in-situ TEM capability can be realized on any standard transmission electron microscopes, and all that needs to be done is to design a special TEM specimen holder, which supplies a desired stimulus to the TEM specimen. These are holder-based in-situ TEM technologies. Column-based technologies like in-situ ETEM and in-situ ion beam irradiation TEM are more favorable when high resolution and multiple external stimuli are desired. The reported in-situ TEM experimental results have shown great impact on materials science and nanoscience and nanotechnology. New insights have been obtained for fundamental microscopic processes, structure-property relationships, catalytic mechanisms, and mechanisms governing materials properties. The more than ever important role of the in-situ TEM in making breakthroughs in scientific and technological R&Ds is stimulating another wave of advancement in electron microscopy after the aberration-corrected TEM.

Acknowledgments Section 3.5.4 was written with major contributions from X. Han, Y. Zhang, K. Zheng, Y. Yue, and Z. Zhang. The author thanks Emily Zhang for helping proof reading.

References

1. NSF Workshop Report on Dynamic in situ electron microscopy as a tool to meet the challenges of the nanoworld, January 3–6, 2006, The Buttes, Tempe, Arizona
2. B.J. Ford, *The Leeuwenhoek Legacy* (Biopress, Bristol, 1991)
3. E. Ruska, Beitrag zur übermikroskopischen Abbildung bei höheren Drucken. Kolloid Z. **100**, 212 (1942)
4. J. Silcox, M.J. Whelan, Direct observations of the annealing of prismatic dislocation loops and of climb of dislocations in quenched aluminum. Philos. Mag. **5**, 1 (1960)
5. N.H. Packan, D.N. Braski, Electron microscope in situ annealing study of voids induced by irradiation in aluminum. J. Nucl. Mater. **34**, 307 (1970)
6. R.T.K. Baker, In situ electron microscopy studies of catalyst particle behavior. Catal. Rev. **19**, 161 (1979)
7. ASU electron microscopy workshop. Microsc. Microanal. **4** (1998)
8. X.F. Zhang, L.C. De Jonghe, Thermal modification of microstructures and grain boundaries in silicon carbide. J. Mater. Res. **18**(12), 2807 (2003)
9. M. Law, X.F. Zhang, R. Yu, T. KuyKendall, P. Yang, Thermally driven interfacial dynamics of metal/oxide bilayer nanoribbons. Small **1**, 1 (2005)
10. R. Yu, H. Song, X.F. Zhang, P. Yang, Thermal wetting of platinum nanocrystals on silica surface. J. Phys. Chem. B **109**, 6940 (2005)
11. S.H. Oh, Y. Kauffmann, C. Scheu, W.D. Kaplan, M. Ruhle, Ordered liquid aluminum at the interface with sapphire. Science **310**, 661 (2005)
12. S.K. Eswaramoorthy, J.M. Howe, G. Muralidharan, In situ determination of the nanoscale chemistry and behavior of solid-liquid systems. Science **318**, 1437 (2007)
13. V.C. Holmberg, M.G. Panthani, B.A. Korgel, Phase transitions, melting dynamics, and solid-state diffusion in a nano test tube. Science **326**, 405 (2009)
14. T. Kamino, H. Saka, A newly developed high resolution hot stage and its application to materials characterization. Microsc. Microanal. Microstruct. **4**, 127 (1993)
15. T. Kamino, T. Yaguchi, H. Saka, In situ study of chemical reaction between silicon and graphite at 1,400°C in a high resolution/analytical electron microscope. J. Electron Microsc. (Tokyo), **43**, 104 (1994)
16. T. Kamino, H. Saka, In-situ HREM heating experiments at very high temperatures. Mat. Res. Soc. Symp. Proc. **404**, 19 (1996)
17. S. Tsukimoto, S. Arai, M. Konno, T. Kamino, K. Sasaki, H. Saka, In situ high resolution electron microscopy/electron energy loss spectroscopy observation of wetting of a Si surface by molten Al. J. Microsc. **203**, 17 (2001)
18. J.G. Lee, H. Mori, In-situ observation of alloy phase formation in nanometre-sized particles in the Sn-Bi system. Philos. Mag. **84**, 2675 (2004)
19. T. Kamino, T. Yaguchi, M. Konno, T. Hashimoto, In situ high temperature TEM observation of interaction between multi-walled carbon nanotube and in situ deposited gold nano-particles. J. Electron Microsc. **54**, 461 (2005)
20. T. Kamino, T. Yaguchi, T. Sato, T. Hashimoto, Development of a technique for high resolution electron microscopic observation of nano-materials at elevated temperatures. J. Electron Microsc. **54**, 505 (2005)
21. T. Akita, K. Tanaka, M. Kohyama, M. Haruta, Analytical TEM study on structural changes of Au particles on cerium oxide using a heating holder. Catal. Today **122**, 233 (2007)
22. H. Saka, T. Kamino, S. Arai, K. Sasaki, In situ heating transmission electron microscopy. MRS Bull. **33**, 93 (2008)
23. T. Tanigagaki, K. Ito, Y. Nagakubo, T. Asakawa, T. Kanemura, An in situ heating TEM analysis method for an interface reaction. J. Electron Microsc. **58**, 281 (2009)
24. T. Kamino, T. Yaguchi, M. Lonno, A. Watabe, Y. Nagakubo, Development of a specimen heating holder with an evaporator and gas injector and its application for catalyst. J. Electron Microsc. **55**, 245 (2006)

25. L.F. Allard, W.C. Biglow, M. Jose-Yacaman, D.P. Nackashi, J. Damiano, S. Mick, A new MEMS-based system for ultra-high-resolution imaging at elevated temperatures. Microsc. Res. Technol. **72**, 208 (2009)
26. Private communication with *Fischione* Instruments
27. T. Kamino, T. Yaguchi, M. Konno, A. Watabe, T. Marukawa, T. Mima, K. Kuroda, H. Saka, S. Arai, H. Makino, Y. Suzuki, K. Kishita, Development of a gas injection/specimen heating holder for use with transmission electron microscope. J. Electron Microsc. **54**, 497 (2005)
28. A. Tonomura, Direct observation of thitherto unobservable quantum phenomena by using electrons. PNAS **102**, 14952 (2005)
29. J. Frank, *Electron Tomography—Three Dimensional Imaging with the Transmission Electron Microscope* (Plenum Press, New York, 1992)
30. K. Dierksen, D. Typke, R. Hegerl, A.J. Koster, W. Baumeister, Towards automatic electron tomography. Ultramicroscopy **40**, 71 (1992)
31. K.H. Downning, H. Sui, M. Auer, Electron tomography: a 3D view of the subcellular world. Anal. Chem. **11**, 7949 (2007)
32. A.M. Glauert, The high voltage electron microscope in biology. J. Cell Biol. **63**, 717 (1974)
33. L. Marton, Bull. Acad. R. Belg. C1. Sci. **21**, 553 (1935)
34. E.P. Butler, K.F. Hale, *Dynamic Experiments in the Electron Microscope* (North-Holland, Amsterdam, 1981)
35. T. Yaguchi, A. Watanabe, Y. Nagakubo, K. Ueda, M. Fukui, T. Kamino, T. Kawasaki, Development of gas environmental cells for in situ TEM applications, in *Proceedings of Microscopy and Microanalysis Annual Meeting*, 8/1-5, 2010, Portland
36. M.J. Flower, High voltage electron microscopy of environmental reactions. J. Microsc. **97**, 171 (1973)
37. P.R. Swann, N.J. Tighe, Jernkont. Annlr. **155**, 251 (1971)
38. P.R. Swann, N.J. Tighe, Performance of differentially pumped environmental cell in the AE1 EM7, in *Proceeding of 5th European Congress on Electron Microscopy*, Manchester (1972), p. 360
39. P.R. Swann, High voltage microscope studies of environmental reaction, in *Electron Microscopy and Structure of Materials*, ed. by G. Thomas, R. Fulrath, R.M. Fisher (University of California Press, Berkeley, 1972), p. 878
40. T.C. Lee, D.K. Dewald, J.A. Eades, I.M. Robertson, H.K. Birnbaum, An environmental cell transmission electron microscopy. Rev. Sci. Instrum. **62**, 1438 (1991)
41. E.D. Boyes, P.L. Gai, Environmental high resolution electron microscopy and applications to chemical science. Ultramicroscopy **67**, 219 (1997)
42. R. Sharma, K. Weiss, Development of a TEM to study in situ structural and chemical changes at an atomic level during gas-solid interactions at elevated temperatures. Microsc. Res. Techniq. **42**, 270 (1998)
43. P.L. Gai, E.D. Boyes, S. Helveg, P.L. Hansen, S. Giorgio, C.R. Henry, Atomic-resolution environmental transmission electron microscopy for probing gas-solid reactions in heterogeneous catalysis. MRS Bull. **32**, 1044 (2007)
44. K. Kishita, H. Sakai, H. Tanaka, H. Saka, K. Kuroda, M. Sakamoto, A. Watabe, T. Kamino, Development of an analytical environmental TEM system and its application. J. Electron. Microsc. **58**, 331 (2009)
45. P.L. Gai, R. Sharma, F.M. Ross, Environmental (S)TEM studies of gas-liquid-solid interactions under reaction conditions. MRS Bull. **33**, 107 (2008)
46. X.F. Zhang, T. Kamino, Imaging gas-solid interactions in an atomic resolution environmental TEM. Microsc. Today **14**, 16 (2006)
47. X.F. Zhang, In-situ gas-heating and real-time 3D imaging: Hitachi H-9500 transmission electron microscope. Am. Lab. **40**, 27 (2008)
48. P.A. Crozier, R. Sharma, A.K. Datye, Oxidation and reduction of small palladium particles on silica. Microsc. Microanal. **4**, 278 (1998)
49. T.W. Hansen, J.B. Wagner, P.L. Hansen, S. Dahl, H. Topsee, C.J.H. Jacobsen, Atomic-resolution in situ transmission electron microscopy of a promoter of a heterogeneous catalyst. Science **294**, 1508 (2001)

50. S. Helveg, C. Lopez-Cartes, J. Hehested, P.L. Hansen, B.S. Calusen, J.R. Rostrup-Nielsen, F. Abild-Pedersen, J.K. Nerskov, Atomic-scale imaging of carbon nanofibre growth. Nature **427**, 426 (2004)
51. J.B. Hannon, S. Kodambaka, F.M. Ross, R.M. Tromp, The influence of the surface migration of gold on the growth of silicon nanowires. Nature **440**, 69 (2006)
52. S. Kodambaka, J. Tersoff, M.C. Reuter, F.M. Ross, Germanium nanowire growth below the eucentric temperature. Science **316**, 729 (2007)
53. B.J. Kim, J. Tersoff, S. Kodambaka, M.C. Reuter, E.A. Stach, F.M. Ross, Kinetics of individual nucleation events observed in nanoscale vapor-liquid-solid growth. Science **322**, 1070 (2008)
54. S. Hofmann, R. Sharma, C.T. Wirth, F. Cervantes-Sodi, C. Ducati, T. Kasama, R.E. Dunin-Borkowski, J. Drucker, P. Bennett, J. Robertson, Ledge-flow-controlled catalyst interface dynamics during Si nanowire growth. Nat. Mater. **7**, 372 (2008)
55. V.P. Oleshko, P.A. Crozier, R.D. Cantrell, A.D. Westwood, J. Electron Microsc. **51**(supplement), S27 (2002)
56. R. Sharma, P. Rez, M. Brown, G.H. Du, M.M.J. Treacy, Nanotechnology **18**, 125602 (2007)
57. M. Haider, H. Rose, S. Uhlemann, B. Kabius, K. Urban, Nature **392**, 768 (1998)
58. N. Dellby, O.L. Krivanek, P.D. Nellist, P.E. Batson, A.R. Lupini, J. Electron Microsc. (Tokyo) **50**, 177 (2001)
59. I.M. Abrams, J.W. McBain, Science **100,** 273 (1944)
60. I.M. Abrams, J.W. McBain, J. Appl. Phys. **15,** 607 (1944)
61. R.T. Joy, The electron microscopical observation of aqueous biological systems. Adv. Opt. Electron Microsc. **5**, 297 (1973)
62. D.F. Parsons, Environmental wet cells for biological medium voltage and high voltage electron microscopy, in *Electron Microscopy* (1973)
63. B. Siegel (ed.), in *Physical Aspects* (Wiley, New York, 1974)
64. D.F. Parsons, Structure of wet specimens in electron microscopy. Science **186**, 407 (1974)
65. M.J. Williamson, R.M. Tromp, P.M. Vereecken, R. Hull, F.M. Ross, Dynamic microscopy of nanoscale cluster growth at the solid-liquid interface. Nat. Mater. **2**, 532 (2003)
66. H. Zheng, R.K. Smith, Y. Jun, C. Kisielowski, U. Dahmen, A.P. Alivisatos, Observation of single colloidal platinum nanocrystal growth trajectories. Science **324**, 1309 (2009)
67. H. Liao, L. Cui, S. Whitelam, H. Zheng, Real-time imaging of Pt_3Fe nanorod growth in solution. Science **336**, 1011 (2012)
68. J.D. Li, M.H. Nielsen, J.R. Lee, C. Frandsen, J.F. Banfield, J. De Yoreo, Direction-specific interactions control crystal growth by oriented attachment. Science **336**, 1014 (2012)
69. J.M. Yuk, J. Park, P. Ercius, K. Kim, D.J. Hellebusch, M.F. Crommie, J.Y. Lee, A. Zettl, A. Alivisatos, High-resolution EM of colloidal nanocrystal growth using graphene liquid cells. Science **336**, 61 (2012)
70. N. de Jonge, D.B. Peckys, G.J. Kremers, D.W. Piston, Electron microscopy of whole cells in liquid with nanometer resolution. Proc. Natl. Acad. Sci. USA **106**(7), 2159–2164 (2009). Epub 2009 Jan 21
71. D.B. Peckys, G.M. Veith, D.C. Joy, N. de Jonge, Nanoscale imaging of whole cells using a liquid enclosure and a scanning transmission electron microscope. Plos One **4**, e8214 (2009)
72. R.C. Moretz, G.G. Hausner, JR., D.F. Parsons, in *Proceedings of the 29th Annual Meeting of the Electron Microscopy Society of America,* Boston, ed. by C.J. Arceneaux (Claitor's, Baton Rouge, 1971), p. 544
73. S.W. Hui, D.F. Parsons, in *Proceedings of the 31th Annual Meeting of the Electron Microscopy Society of America,* New Orleans, ed. by C.J. Arceneaux (Claitor's, Baton Rouge, 1973), p. 340
74. P.L. Gai, Development of wet environmental TEM (Wet-ETEM) for in situ studies of liquid-catalyst reactions on the nanoscale. Microsc. Microanal. **8**, 21 (2002)
75. P.W. Sutter, E.A. Sutter, Dispensing and surface-induced crystallization of aeptolitre liquid metal-alloy drops. Nat. Mater. **6**, 363 (2007)
76. J.Y. Huang, S. Ceh, Z.Q. Wang, K. Kempa, Y.M. Wang, S.H. Jo, G. Chen, M.S. Dresselhaus, Z.F. Ren, Superplastic carbon nanotubes. Nature **439**, 281 (2006)

77. J.Y. Huang, S. Chen, Z.F. Ren, Z. Wang, K. Kempa, M.J. Naughton, G. Chen, M.S. Dresselhaus, Enhanced ductile behavior of tensile-elongated individual double-walled and triple-walled carbon nanotubes at high temperatures. Phys. Rev. Lett. **98**, 185501-1 (2007)
78. J.Y. Huang, S. Chen, Z.F. Ren, G. Chen, M.S. Dresselhaus, Real-time observation of tubule formation from amorphous carbon nanowires under high-bias Joule heating. Nano Lett. **6**, 1699 (2006)
79. B.C. Regan, S. Aloni, R.O. Ritchie, U. Dahmen, A. Zettl, Carbon nanotubes as nanoscale mass conveyors. Nature **428**, 924 (2004)
80. A. Barreiro, R. Rurali, E.R. Hernandez, J. Moser, T. Pichler, L. Forro, A. Bachtold, Subnanometer motion of cargoes driven by thermal gradiants along carbon nanotubes. Science **320**, 775 (2008)
81. J. Cumings, P.G. Collins, A. Zettl, Peeling and sharpening multiwall nanotubes. Nature **406**, 586 (2000)
82. J. Cumings, A. Zettl, Low-friction nanoscale linear bearing realized from multiwall carbon nanotubes. Science **289**, 602 (2000)
83. P. Gao, Z. Kang, W. Fu, W. Wang, X. Bai, E. Wang, Electrically driven redox process in cerium oxides. J. Am. Chem. Soc. **132**, 4197 (2010)
84. P. Poncharal, C. Berger, Y. Yi, Z.L. Wang, W.A. de Heer, Room temperature ballistic conduction in carbon nanotubes. J. Phys. Chem. B **106**, 12104 (2002)
85. M.S. Wang, J. Wang, Q. Chen, L.M. Peng, Fabrication and electrical and mechanical properties of carbon nanotube interconnections. Adv. Funct. Mater. **15**, 1825 (2005)
86. M.S. Wang, L.M. Peng, J.Y. Wang, Q. Chen, Shaping carbon nanotubes and effects on their electrical and mechanical properties. Adv. Funct. Mater. **16**, 1462 (2006)
87. K.H. Liu, P. Gao, Z. Xu, X.D. Bai, E.G. Wang, In situ probing electrical response on bending of ZnO nanowires inside transmission electron microscope. Appl. Phys. Lett. **92**, 213105-1 (2008)
88. M.S. Wang, Q. Chen, L.M. Peng, Field-emission characteristics of individual carbon nanotubes with a conical tip: the validity of the Fowler-Nordheim theory and maximum emission current. Small **4**, 1907 (2008)
89. M.S. Wang, Q. Chen, L.M. Peng, Grinding a nanotube. Adv. Mater. **20**, 724 (2008)
90. A.N. Chiaramonti, L.J. Thompson, W.F. Egelhoff, B.C. Kabius, A.K. Petford-Long, In situ TEM studies of local transport and structure in nanoscale multilayer films. Ultramicroscopy **108**, 1529 (2008)
91. A.N. Chiaramonti, D.K. Schreiber, W.F. Egelhoff, D.N. Seidman, A.K. Petford-Long, Effects of annealing on local composition and electrical transport correlations in MgO-based magnetic tunnel junctions. Appl. Phys. Lett. **93**, 103113-1 (2008)
92. J.W. Lau, P. Morrow, J.C. Read, V. Höink, W.F. Egelhoff, L. Huang, Y. Zhu, In situ tunneling measurements in a transmission electron microscope on nanomagnetic tunnel junctions. Appl. Phys. Lett. **96**, 262508-1 (2010)
93. J.Y. Huang, L. Zhong, C.M. Wang, J.P. Sullivan, W. Xu, L.Q. Zhang, S.X. Mao, N.S. Hudak, X.H. Liu, A. Subramanian, H. Fan, L. Qi, J. Li, In situ observation of the electrochemical lithiation of a single SnO_2 nanowire electrode. Science **330**, 1515 (2010)
94. T. Fujieda, K. Hidaka, M. Hayashibara, T. Kamino, H. Matsumoto, Y. Ose, H. Abe, T. Shimizu, H. Tokumoto, In situ observation of field emission from an individual carbon nanotube by Lorenz microscopy. Appl. Phys. Lett. **85**, 5739 (2004)
95. T. Fujieda, K. Hidaka, M. Hayashibara, T. Kamino, Y. Ose, H. Abe, T. Shimizu, H. Tokumoto, Direct observation of field emission sites in the single multiwalled carbon nanotube by Lorenz microscopy. Jpn. J. Appl. Phys. **44**, 1661 (2005)
96. T. Fujieda, M. Okai, K. Hidaka, H. Matsumoto, H. Tokumoto, Behavior of catalyst particle at tip of carbon nanotube during field emission. Appl. Phys. Express **1**, 014002-1 (2008)
97. K. Liu, W. Wang, Z. Xu, X. Bai, E. Wang, Y. Yao, J. Zhang, Z. Liu, Chirality-dependent transport properties of double-walled nanotubes measured in situ on their field-effect transistors. J. Am. Chem. Soc. **131**, 62 (2009)
98. Z.W. Shan, G. Adesso, A. Cabot, M.P. Sherburne, S.A. Syed Aasif, O.L. Warren, D.C. Chrzan, A.M. Minor, A.P. Alivisatos, Ultrahigh stress and strain in hierarchically structured hollow nanoparticles. Nat. Mater. **7**, 947 (2008)

99. N. Gane, F.P. Bowden, J. Appl. Phys. **39**, 1432 (1968)
100. N. Gane, Proc. R. Soc. Lond. Ser. A **317**, 367 (1970)
101. M. Legros, D.S. Gianola, C. Motz, Quantitative in situ mechanical testing in electron microscopes. MRS Bull. **35**, 354 (2010)
102. P. Poncharal, Z.L. Wang, D. Ugart, W.A. de Heer, Electrostatic deflections and electromechanical resonances of carbon nanotubes. Science **283**, 1513 (1999)
103. H.G.F. Wilsdorf, ASTM Spec. Technol. **245**, 43 (1958)
104. U. Messerschmidt, F. Appel, Ultramicroscopy **1**, 223 (1976)
105. E.P. Butler, Rep. Prog. Phys. **42**, 833 (1979)
106. I.M. Robertson, P.J. Ferreira, G. Dehm, R. Hull, E.A. Stach, Visualizing the behavior of dislocations—seeing is believing. MRS Bull. **33**, 122 (2008)
107. I.M. Robertson, H.K. Birnbaum, P. Sofronis, Hydrogen effects on plasticity, in *Dislocations in Solids*, ed. by J. P. Hirth, L. Kubin (Elsevier B.V, Netherlands, 2009), pp. 249–293
108. Z.W. Shan, E.A. Stach, J.M.K. Wiezorek, J.A. Knapp, D.M. Follstaedt, S.X. Mao, Grain boundary-mediated plasticity in nanocrystalline nickel. Science **305**, 654 (2004)
109. Z.W. Shan, J.M.K. Wiezorek, E.A. Stach, D.M. Follstaedt, J.A. Knapp, S.X. Mao, Dislocation dynamics in nanocrystalline nickel. Phys. Rev. Lett. **98**, 095502-1 (2007)
110. Z.W. Shan, J.A. Knapp, D.M. Follstaedt, E.A. Stach, J.M.K. Wiezorek, S.X. Mao, Inter- and intra-agglomerate fracture in nanocrystalline nickel. Phys. Rev. Lett. **100**, 105502-1 (2008)
111. M.A. Haque, H.D. Espinosa, H.J. Lee, MEMS for in situ testing—Handling, actuation, loading, and displacement measurements. MRS Bull. **35**, 375 (2010)
112. B. Peng, M. Locascio, P. Zapol, S.Y. Li, S.L. Mielke, G.C. Schatz, H.D. Espinosa, Measurements of near-ultimate strength for multiwalled carbon nanotubes and irradiation-induced crosslinking improvements. Nat. Nanotechnol. **3**, 626 (2008)
113. M. Locascio, B. Peng, P. Zapol, Y. Zhu, S.Y. Li, S.L. Mielke, T. Belytschko, H.D. Espinosa, Exp. Mech. **49**, 169 (2009)
114. Z.W. Shan, R.K. Mishra, S.A.S. Asif, O.L. Warren, A.M. Minor, Mechanical annealing and source-limited deformation in submicrometer-diameter Ni crystals. Nat. Mater. **7**, 115 (2007)
115. M.S. Wang, I. Kaplan-Ashirl, X.L. Wei, R. Rosentsveig, H.D. Wagner, R. Tenne, L.M. Peng, In situ TEM measurements of the mechanical properties and behavior of WS2 nanotubes. Nano Res. **1**, 22 (2008)
116. Q. Yu, Z.W. Shan, J. Li, X.X. Huang, L. Xiao, J. Sun, E. Ma, Strong crystal size effect on deformation twinning. Nature **463**, 335 (2010)
117. X.D. Han, K. Zheng, Y.F. Zhang, X.N. Zhang, Z. Zhang, Z.L. Wang, Low temperature in situ large strain plasticity of silicon nanowires. Adv. Mater. **19**, 2112 (2007)
118. Y.F. Zhang, X.D. Han, K. Zheng, Z. Zhang, X.N. Zhang, J.Y. Fu, Y. Ji, Y.J Hao, X.Y. Guo, Z.L. Wang, Direct observation of super-plasticity of beta-SiC nanowires at low temperature. Adv. Funct. Mater. **17**, 3435 (2007)
119. K. Zheng, C.C. Wang, Y.Q. Cheng, Y.H. Yue, X.D. Han, Z. Zhang, Z.W. Shan, S.X. Mao, M.M. Ye, Y.D. Yin, E. Ma, Electron-beam-assisted superplastic shaping of nanoscale amorphous silica. Nat. Commun. **1**, 1 (2010)
120. X.D. Han, Y.F. Zhang, K. Zheng, X.N. Zhang, Z. Zhang, Y.J. Hao, X.Y. Guo, J. Yuan, Z.L. Wang, Direct observation of super-plasticity of beta-SiC nanowires at low temperature. Nano Lett. **7**, 452 (2007)
121. K. Zheng, X.D. Han, L.H. Wang, Y.H. Yue, Y.F. Zhang, Y. Qin, X.N. Zhang, Z. Zhang, Atomic mechanisms governing the elastic limit and the incipient plasticity of bending Si nanowires. Nano Lett. **9**, 2471 (2009)
122. X.D. Han, Y.F. Zhang, X.Q. Liu, Z. Zhang, Y.J. Hao, X.Y. Guo, Lattice bending, disordering and amorphization induced plastic deformation in a SiC nanowire. J. Appl. Phys. **98**, 124307-1 (2005)
123. J.H. Wang, S. Yip, S.R. Phillpot, D. Wolf, Crystal instabilities at finite strain. Phys. Rev. Lett. **71**, 4182 (1993)

124. L. Sun, F. Banhart, A.V. Krasheninnikov, J.A. Rodriguez-Manzo, M. Terrones, P.M. Ajayan, Carbon nanotubes as high pressure cylinders and nanoextruders. Science **312**, 1199 (2006)
125. J. Cumings, E. Olsson, A.K. Petford-Long, Y. Zhu, Electric and magnetic phenomena studied by in situ transmission electron microscopy. MRS Bull. **33**, 101 (2008)
126. C. Tsuruta, T. Kamino, H. Sato, *Observation of magnetic domain in cobalt thin foil*, Hitachi Technical Data, Sheet No. 51
127. T. Hirayama, Q. Ru, T. Tanji, A. Tonomura, Observation of magnetic-domain states of barium ferrite particles by electron holography. Appl. Phys. Lett. **63**, 418 (1993)
128. J.J. Kim, A. Tonomura, K. Hirata, Y. Ishida, D. Shindo, M. Takahashi, Magnetic domain observation in writer pole tip for perpendicular recording head by electron holography. Appl. Phys. Lett. **92**, 162501 (2008)
129. A. Sugawara, K. Fukunaga, M.R. Scheinfein, H. Kobayashi, H. Kitagawa, A. Tonomura, Electron holography study of the temperature variation of the magnetic order parameter within circularly nickel nanoparticle rings. Appl. Phys. Lett. **91**, 262513 (2007)
130. A. Sugawara, T. Akashi, P.D. Brown, R.P. Campion, T. Yoshida, B.L. Gallagher, A. Tonomura, High-resolution observations of temperature-dependent magnetic domain structures within $Ga_xMn_{1-x}As$ by Lorentz microscopy. Phys. Rev. B **75**, 241306-1 (2007)
131. K. Fukunaga, A. Sugawara, Anisotropic cross-tie wall and their confinement in self organized undulating Fe film. J. Appl. Phys. **103**, 053909 (2008)
132. A. Sugawara, H. Kasai, A. Tonomura, P.D. Brown, R.P. Campion, K.W. Edmonds, B.L. Gallagher, J. Zemen, T. Jungwirth, Domain walls in the (Ga, Mn) As diluted magnetic semiconductor. Phys. Rev. Lett. **100**, 047202 (2008)
133. A.C. Twitchett, R.E. Dunin-Borkoski, P.A. Midgley, Philos. Mag. **86**, 5805 (2006)
134. A. Tonomura, *The Quantum World Unveiled by Electron Waves* (World Scientific, Singapore, 2008)
135. H. Lichte, M. Lehmann, Electron holography—basics and applications. Rep. Prog. Phys. **70**, 1 (2007)
136. R.E. Dunin-Boekowski, T. Kasama, A. Wei, S.L. Tripp, M.J. Hytch, E. Snoeck, R.J. Harrison, A. Putnis, Off-axis electron holography of magnetic nanowires and chains, rings, and plannar arrays of magnetic nanoparticles. Microsc. Res. Technol. **64**, 390 (2004)
137. Y. Togawa, K. Harada, T. Akashi, H. Kasai, T. Matsuda, F. Nori, A. Maeda, A. Tonomura, Direct observation of rectified motion of vortices in a niobium superconductor. Phys. Rev. Lett. **95**, 087002 (2005)
138. Y. Togawa, T. Kimura, K. Harada, T. Akashi, T. Matsuda, A. Tonomura, Y. Otani, Current-excited magnetization dynamics in narrow ferromagnetic wires. Jpn. J. Appl. Phys. (Express) **45**, L683 (2006)
139. Y. Togawa, T. Kimura, K. Harada, T. Akashi, T. Matsuda, A. Tonomura, Y. Otani, Current-excited magnetization reversal under in-plane magnetic field in a nano-scaled ferromagnetic wire. Appl. Phys. Lett. **92**, 012505 (2008)
140. Y. Togawa, K. Harada, T. Akashi, H. Kasai, T. Matsuda, A. Maeda, A. Tonomura, Rectified motion of vortices in a niobium superconductor observed by Lorentz microscopy. Physica C **426–431**, 141 (2005)
141. A. Tonomura, H. Kasai, O. Kamimura, T. Matsuda, K. Harada, T. Yoshida, T. Akashi, J. Shimoyama, K. Kishio, T. Hanaguri, K. Kitazawa, T. Masui, S. Tajima, N. Koshizuka, P.L. Gammel, D. Bishop, M. Sasase, S. Okayasu, Observation of structures of chain vortices inside anisotropic high-T_c superconductors. Phys. Rev. Lett. **88**, 237001 (2002)
142. R.E. Dunin-Borkowski, M.R. McCartney, D.J. Smith, S.S.P. Parkin, Towards quantitative electron holography of magnetic thin films using in situ magnetization reversal. Ultramicroscopy **74**, 61 (1998)
143. J.W. Lau, M. Beleggia, M.A. Schofield, G.F. Neumark, Y. Zhu, Direct correlation of reversal rate dynamics to domain configurations in micron-sized permalloy elements. J. Appl. Phys. **97**, 10E702-1 (2005)

144. J.W. Lau, M. Beleggia, Y. Zhu, Common reversal mechanisms and correlation between transient domain states and field sweep rate in patterned Permalloy structures. J. Appl. Phys. **102**, 043906-1 (2007)
145. Z. Akase, D. Shindo, In situ Lorentz microscopy in an alternating magnetic field. J. Electron Microsc. **59**, 207 (2010)
146. A. Lenk, H. Lichte, U. Muehle, J. Electron Microsc. **54**, 351 (2005)
147. S. Frabboni, G. Matteucci, G. Pozzi, M. Vanzi, Phys. Rev. Lett. **55**, 2196 (1985)
148. W.D. Rau, P. Schwander, F.H. Baumann, W. Hoppner, A. Ourmazd, Phys. Rev. Lett. **82**, 2614 (1999)
149. A.C. Twitchett, R.E. Dunin-Bokowski, P.A. Midgley, Phys. Rev. Lett. **88**, 238302 (2002)
150. A.C. Twitchett, R.E. Dunin-Bokowski, R.F. Broom, P.A. Midgley, J. Phys. Condens. Matter **16**, S181 (2004)
151. A.C. Twitchett-Harrison, T.J.V. Yates, S.B. Newcomb, R.E. Dunin-Borkowski, P.A. Midgley, Nano Lett. **7**, 2020 (2007)
152. A.C. Twitchett, R.E. Dunin-Borkowski, R.J. Hallifax, R.F. Broom, P.A. Midgley, Microsc. Microanal. **11**, 1 (2005)
153. X. Portier, E.Y. Tsymbal, A.K. Petford-Long, T.C. Anthony, J.A. Brug, Phys. Rev. B. **58**, R591 (1998)
154. F. Junginger, M. Klaui, D. Backes, U. Rudiger, T. Kasama, R.E. Dunin-Borkoski, L.J. Heyderman, C.A.F. Vaz, J.A.C. Bland, Appl. Phys. Lett. **90**, 132506 (2007)
155. M. Hayashi, L. Thomas, R. Moriya, C. Rettner, S.P. Parkin, Current-controlled magnetic domain-wall nanowire shift register. Science **320**, 209 (2008)
156. L. Huang, M.A. Schofield, Y. Zhu, Direct observation of the controlled magnetization reversal processes in Py/Al/Py asymmetric ring stacks. Appl. Phys. Lett. **95**, 042501-1 (2009)
157. L. Huang, M.A. Schofield, Y. Zhu, Control of double-vortex domain configurations in a shape-engineered trilayer nanomagnet system. Adv. Mater. **22**, 492 (2010)
158. T. Uhlig, M. Heumnann, J. Zweck, Development of a specimen holder for in situ generation of pure in-plane magnetic fields in a transmission electron microscope. Ultramicroscopy **94**, 193 (2003)
159. M. Inoue, T. Tomita, M. Naruse, Z. Aakase, Y. Murakami, D. Shindo, Development of a magnetizing stage for in situ observations with electron holography and Lorentz microscopy. J. Electron Microsc. **54**, 509 (2005)
160. J.W. Lau, J.K. Bording, M. Beleggia, Y. Zhu, Energy barrier to magnetic vortex nucleation. Appl. Phys. Lett. **88**, 012508-1 (2006)
161. L. Huang, Y. Zhu, Controlled reversal of coupled Néel walls in flux-closure magnetic trilayer elements. Appl. Phys. Lett. **95**, 222502-1 (2009)
162. X.Z. Yu, Y. Onose, N. Kanazawa, J.H. Park, J.H. Han, Y. Matsui, N. Nagaosa, Y. Tokura, Real-space observation of a two-dimensional skyrmion crystal. Nature **465**, 901–904 (2010)
163. D. Shindo, Y.G. Park, Y. Gao, H.S. Park, Electron holography of Fe-based nanocrystalline magnetic materials. J. Appl. Phys. **95**, 6521 (2004)
164. H.S. Park, Y.G. Park, Y. Gao, D Shindo, M. Inoue, Direct observation of magnetization reversal in thin Nd2Fe14B film. J. Appl. Phys. **97**, 033908 (2005)
165. J.W. Lau, M.A. Schofield, Y. Zhu, A straightforward specimen holder modification for remnant magnetic-field measurement in TEM. Ultramicroscopy **107**, 396 (2007)
166. J. Cumings, A. Zettl, M.R. McCartney, J.C.H. Spence, Electron holography of field-emitting carbon nanotubes. Phys. Rev. Lett. **88**, 056804-1 (2002)
167. J. Cumings, A. Zettl, M.R. McCartney, Carbon nanotube electrostatic biprism: principle of operation and proof of concept. Microsc. Microanal. **10**, 420 (2004)
168. D.W. Pashley, A.E.B. Presland, Ion damage to metal films inside an electron microscope. Philos. Mag. **6**, 1003 (1961)
169. J.A. Hinks, A review of transmission electron microscopes with in situ ion irradiation. Nucl. Instrum. Methods Phys. Res. B **267**, 3652 (2009)

170. Y. Yan, Swift heavy ion irradiation damage in $YBa_2Cu_3O_{7-d}$ superconductors, in *Progress in Transmission Electron Microscopy, II. Applications in Materials Science*, ed. by X.F. Zhang, Z. Zhang (Springer/Tsinghua University Press, Berlin/Beijing, 2001), pp. 213–245
171. T. Tanigagaki, K. Ito, Y. Nagakubo, T. Asakawa, T. Kanemura, An in situ heating TEM analysis method for an interface reaction. J. Electron Microsc. **58**, 281 (2009)
172. R.F. Egerton, P. Li, M. Malac, Radiation damage in the TEM and SEM. Micron **35**, 399 (2004)
173. P.B. Hirsch, R.W. Horne, M.J. Whelan, Direct observations of the arrangement and motion of dislocations in aluminum. Philos. Mag. A **1**, 677 (1956)
174. P.B. Hirsch, Direct observations of moving dislocations: reflections on the thirtieth anniversary of the first recorded observations of moving dislocations by transmission electron microscopy. Mater. Sci. Eng. **84**, 1 (1986)
175. D.W. Pashley, M.J. Stowell, M.H. Jacobs, T.J. Law, The growth and structure of gold and silver deposits formed by evaporation inside an electron microscope. Philos. Mag. **10**, 127 (1964)
176. R. Sinclair, T. Yamashita, F.A. Ponce, Atomic motion on the surface of a cadmium telluride single crystal. Nature **290**, 386 (1981)
177. B.J. Kooi, JThM De Hosson, On the crystallization of thin films composed of $Sb_{3.6}Te$ with Ge for rewritable data storage. J. Appl. Phys. **95**, 4714 (2004)
178. O. Kamimura, T. Dobashi, K. Kawahara, T. Abe, K. Gohara, 10-kV diffractive Imaging using newly developed electron diffraction microscope. Ultramicroscopy **110**, 130 (2010)
179. A. Zobelli, A. Gloter, C.P. Ewels, G. Seifert, C. Colliex, Electron knock-on cross section of carbon and boron nitride nanotubes. Phys. Rev. B **75**, 245402 (2007)
180. F. Banhart, P.M. Ajayan, Carbon onions as nanoscopic pressure cells for diamond formation. Nature **382**, 433 (1996)
181. M. Pan, Developing image detectors for in situ TEM applications. J. Chin. Electron Microsc. Soc. **29**, 295 (2010)